Clogging caused by particle migration during groundwater recharge in uncemented sandstone reservoir

F. J. Yang[1, 2], G. L. Wang[3], H. J. Liu[1, 2], D. W. Hu[1, 2*], H. Zhou[1, 2]

[1] State Key Laboratory of Geomechanics and Geotechnical Engineering, Institute of Rock and Soil Mechanics, Chinese Academy of Sciences, Wuhan 430071, China.

[2] University of Chinese Academy of Sciences, Beijing 100049 China.

[3] Institute of Hydrogeology and Environmental Geology, Chinese Academy of Geological Sciences, Shijiazhuang, Hebei 050061, China.

Corresponding author: Dawei Hu (dwhu@whrsm.ac.cn)

Key Points:

- Clogging caused by coupling effect of in-situ stress and grain-migration during groundwater recharge for uncemented sandstone
- In-situ stress and pore pressure are key factors controlling the failure of uncemented sandstone, but excluding grain composition
- Absolute permeability decreases with the increased grain size due to the crushing effect of in-situ stress and the grain migration

Abstract

Clogging caused by grain migration during groundwater recharge is a critical problem for long-term operation period of Ground water-source heat pump (GWHP), especially for uncemented sandstone reservoir. Thus, the permeability tests of three groups of uncemented sandstone samples with different grain compositions are carried out respectively, under in-situ stress. The clogging caused by coupling effect of in-situ stress and grain-migration during groundwater recharge for uncemented sandstone. Firstly, the original grains are crushed even broken into fine grain under in-situ stress. Then, the fine grains originally filled or secondary crushed migrate along the space between skeleton structure and gradually deposit at the bottom of samples, resulting in the increase in pore pressure and the decrease in apparent permeability, which is in good agreement with the observations in the field. Apparent permeability exhibits different variation duo to the differences in grain composition, whilst the absolute permeability decreases with the increased grain size due to the compaction effect or/and the grain migration. Furthermore, the pore pressure increases with flow rate and tends to 1/2 of applied hydrostatic stress till the failure of samples. This indicates in-situ stress and pore pressure are key factors controlling the failure of uncemented sandstone, but excluding grain composition. The testing results in this context could facilitate our understanding of the clogging caused by coupling effect of in-situ stress and grain-migration during groundwater recharge for uncemented sandstone, and some suggestions could be provided for the utilization of hydrothermal geothermal energy especially for the uncemented sandstone reservoir.

Key words: Ground Water-Source Heat Pump; Clogging; Grain Migration; Groundwater recharge; Uncemented Sandstone

1 Introduction

As the depletion of fossil fuels such as coal, petroleum, natural gas etc, the energy problems have been becoming a serious problem (Lior 2008, 2010). Simultaneously, the assumption of fossil energy havs caused many environmental problems, including air pollution, water pollution, global warming etc (Cheng et al., 2016). Therefore, it is imperative to develop the new renewable and green energy, making the geothermal energy attracts more and more attentions (Barbier, 2002; Lior 2008, 2010; Zhu et al., 2015; Chen and Jiang, 2015; Zhao et al., 2015; , Li et al., 2015; Caulk & Tomac, 2017; Lei et al., 2019). Ground water-source heat pump (GWHP) are identified as effective for reducing the energy demand and consumption (Hughes and Muessel, 2000), and it is a clean and renewable technology. GWHPs have the most potential for supplying the energy needs of future cities (Bayer et al., 2012). It has been widely used in countries such as the US, UK, China, Sweden and Japan (Lund, 2009). However, GWHPs are still facing challenges in technology application such as groundwater recession, water reinjection, corrosion and clogging problem (Stáhl et al., 2000; Nian et al., 2018b, 2019). Especially, the clogging is a serious problem during groundwater recharge in the GWHP system (Chen et al., 2017; Chu et al., 2019), which causes a low reinjection efficiency. In some cases, it is necessary to retrofit the recharge wells, or even to abandon them (Rinck-Pfeiffer et al., 2000), causing financial constraints, water waste, and groundwater recession, which strongly restricts the development and utilization of hydrothermal geothermal energy (Tufenkji, 2007).

Clogging of groundwater recharge is mainly caused by suspended particles (Rehg et al., 2005; Katarzyna, 2006; Wang et al., 2018b;), chemical sedimentation (Xu et al., 2011; Bustos

Medina et al., 2013; Cui et al., 2018), microorganism/ bacteria growth (Chapelle, 1992; Baveye et al., 1998; Xian et al., 2019), production of extracellular polymeric substances (Xia et al., 2016), entrapment of gas (Ye et al., 2009). Previous investigations have indicated that the physical clogging caused by suspended particles is a dominant contributor, accounting for more than 50% of all factors (Pavelic et al., 1998, 2011; Bradford et al., 2015; Torkzaban et al. 2015), the properties of the suspended particles (such as concentration, particle size and the diameter ratio of particle) play a crucial role in the clogging process (Pavelic et al., 2007). In addition, biological factors such as microbial growth and bacteria are second-most important cause of clogging during groundwater recharge, and extracellular polymeric substances produced by microbial metabolism also contributes to biological clogging (Xia et al., 2014). Suleiman and Swartzendruber (2003) found that hydraulic conductivity was reduced by two orders of magnitude when the content of bacteria exceeded 1.3 × 106 CFU/g. The chemical clogging caused by mineral sedimentation and colloid release is also an indispensable component of recharge clogging (Xu et al., 2011; Bustos Medina et al., 2013), accounting for 15%. The factors such as the dissolved oxygen, pH and the content of metal cation (ferrous ion, calcium ion) play an important role in the chemical clogging (Xu et al., 2016; Van Beek et al., 2017; Li et al., 2019).

Weak-cemented and uncemented sandstone reservoir is the common geological conditions for the development and utilization of hydrothermal geothermal energy (Chen et al., 2017; Chu et al., 2019). A direct reflection of the clogging of weak-cemented and uncemented sandstone is the variation in permeability (Baveye et al., 1998; Reddi et al., 2005; Deo et al., 2010; Xu et al., 2016; Zheng et al., 2020). Thus, various factors affecting the permeability characteristics of the weak-cemented and uncemented sandstone have been investigated under unconfined stress or low confining stress, e.g. compaction, porosity, pore size, temperature and clay minerals, etc (Houseknecht, 1989; Schutjens et al., 1996; AlHomadhi, 2014; Barnaji et al., 2016; Huo and Benson, 2016; Kim and Lee, 2017; Xiong et al. 2018a, 2018b). However, the clogging caused by grain migration are rarely reported, to the authors' knowledge, especially for the weak-cemented and uncemented sandstone reservoir, where grain migration is serious during groundwater recharge. Futhermore, in-situ stress is a factor that cannot be ignored for the development and utilization of hydrothermal geothermal energy especially for the extraction of higher temperature groundwater (Templeton et al., 2014; Nian and Cheng, 2018a). For this, the coupling effect of in-situ stress and grain-migration on clogging during the groundwater recharge for the weak-cemented and uncemented sandstone reservoir are investigated in this paper. In addition, the grain composition has a significant effect on the transportation properties of weak-cemented and uncemented sandstone (Masch and Denny, 1966; Rosas et al., 2014; AlHomadhi, 2014; and Wang et al., 2017a, 2019a). Thus, the permeability tests of three groups of samples with different grain compositions under different flow rate are carried out respectively, under in-situ stress.

2 Materials and Methods

2.1 Background of a geothermal field in the uncemented sandstone reservoirs

Jianghan oilfield, where the abundant geothermal resources can be utilized, especially for the hydrothermal geothermal energy, is located in Hubei Province, China. Statistics show that there are more than 2,500 abandoned oilfield wells in JiangHan oilfield till 2016, which presents an interesting opportunity to be retrofitted as a geothermal system as they are generally deep enough to access high temperature (Cheng et al., 2014). The Neogene Guanghuasi formation,

with burial depths of 600–700 m and a poor cementation, is composed of uncemented sandstone, which is overlaid by Quaternary sedimentary formations. The porosity ranges from 24.9% to 43.8% and the mean porosity is 36.5%. The pressure coefficient (i.e., the ratio of initial pore pressure to the hydrostatic stress of the stratum) is about 1.0, implying that the uncemented sandstone reservoir is a normal pressure system. The properties of the uncemented sandstone reservoir is shown in Table 1. Up to now, the Jianghan oilfield owns the largest GWHP system in Central China. However, the decline in the efficiency of geothermal water recharge has become a serious challenge, which has become a threat to the long-term operation of the GWHP systems. Therefore, it is necessary to understand the permeability characteristics and the clogging mechanism of uncemented sandstone reservoirs during groundwater recharge under in-situ stress.

Table 1 Physical properties of the geothermal reservoir

In-situ stress (MPa)	Formation pressure coefficient	Grains density (g/cm^3)	Saturated density (g/cm^3)	Porosity %
12.5	1.0	2.7	2.2	36.5

2.2 Experimental material

The uncemented sandstone obtained from the Guanghuasi formation of Jianghan oilfield, is mainly composed of four types of minerals include albite (39.69%), quartz (24.50%), biotite (12.99%) and micro-plagioclase (22.82%), etc. The uncemented sandstone is characterized as argillaceous cementation and low cementation degree (Figure 1), and the grain size distribution is shown in Figure 2. The cylindrical samples with the diameter of 50 mm and the length of 100 mm are prepared for the permeability tests based on the reservoir conditions include the water content, density and porosity. The sandstone samples, wrapped using a thermal shrinkable tube, are saturated with the sterilized distilled water using H15558 vacuum pump for 24 hours (the accuracy is ± 0.25%).

Figure 1 Uncemented sandstone specimens taken from the Guanghuasi formation in the Jianghan oilfield

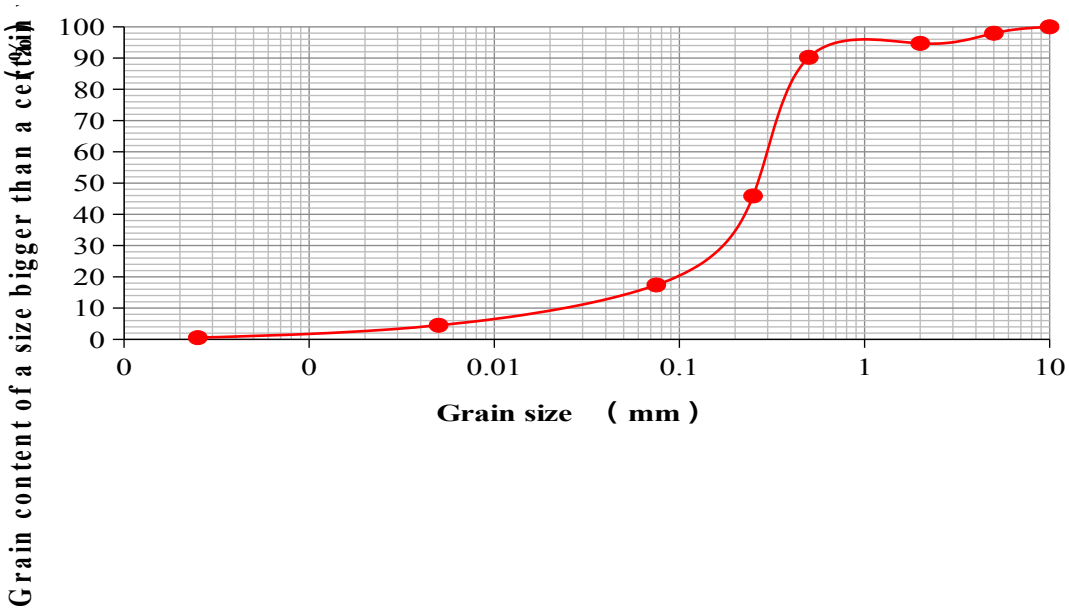

Figure 2 Grain size distribution of uncemented sandstone

2.3 Testing scheme

This work mainly focus on the coupling effect of in-situ stress and grain-migration on clogging during groundwater recharge for uncemented sandstone reservoisr, and the effect of grain composition and flow rate on the transportation properties. Thus, the permeability tests are carried out on three groups of samples with different grain compositions, i.e., Single Grain Size (SGS), Dual Grain Size (DGS) and Natural Gradation (NG) under in-situ stress. The experimenatal work is divided into four steps. Firstly, the uncemented sandstone obtained from the Guanghuasi formation is dried to a constant weight, then the dried uncemented sandstone are divided into six groups based on the grain size, followed by the preparation of sample according to the water content, density and porosity in uncemented sandstone reservoirs, and finally the permeability of uncemented sandstone with SGS, TGS and NG under in-situ stress are measured.

2.4 Sample preparation

The uncemented sandstone obtained from the Jianghan oilfield is dried to a constant weight under the temperature of 105 °C using XL101-3 drying oven (the accuracy is ±1°C). Then, the dried uncemented sandstone is divided into six groups as shown in Table 2, using the standard test sieve (National Standard (China): GB/T6003.1-2012) with the mesh size equal to 0.075 mm, 0.25 mm, 0.5 mm, 1.0 mm, 2.0 mm and 5.0 mm respectively.

The cylindrical samples consisting of SGS, DGS and NG are prepared for the permeability tests according to the density, water content and porosity of uncemented sandstone reservoirs. Firstly, the weight of dry sand and water required for a sample that has similar properties (e.g. density, porosity and water content) with the uncemented sandstone reservoir is calculated by equations (1)-(5). Then, the dry sand and the sterilized distilled water are evenly mixed in a glass container, and are placed in a mold with a diameter of 50 mm and the length of 150 mm. Finally, the mold is placed on a compression testing machine, where the machine is loaded in displacement mode until the prepared sample height is equal to 100 mm. The force is kept stable until the sample height does not rebound, so that a standard sample with a diameter of 50 mm

and the length of 100 mm is prepared. The sample preparation process is shown in Figure 3, the preparation curve is shown in Figure 4, and the physical parameters of prepared samples are shown in Table 3. In addition, the prepared samples are water-saturated using the H15558 vacuum pump (accuracy of ±0.25%) for 24 h. The specimens are wrapped using a thermal shrinkable tube to prevent the contact with water.

$$n = \left(\rho_s - \rho_{rs} \right) / \rho_s \times 100\% \tag{1}$$

where n is the porosity of the geothermal reservoirs, 36.5 %; ρ_s is the density of solid grains of uncemented sandstone, 2.7 g/cm^3; ρ_{rs} is the unit weight of the prepared sample of uncemented sandstone, g/cm^3.

$$\rho_{rs} = \rho / (1 + \omega) \tag{2}$$

where ρ is the density of the geothermal reservoirs, 2.1 g/cm^3; ω is the water content of the prepared uncemented sandstone sample, %.

$$\omega = m_{wat} / m_s \times 100\% \tag{3}$$

where m_{wat} is the water mass of the prepared sample, g; m_s is the mass of solid grains of the prepared sample, g.

$$m = m_{wat} + m_s \tag{4}$$

where m is the mass of the prepared uncemented sandstone sample, g;

$$\rho = m / V \tag{5}$$

where V is the volume of the prepared uncemented sandstone sample 196.35 cm^3.

Table 2 Classification of grain size

Groups	I	II	III	IV	V	VI
Grain size (mm)	<0.075	0.075 ~ 0.25	0.25 ~ 0.5	0.5 ~ 1	1 ~ 2	2 ~ 5

Table 3 Physical parameters of the prepared uncemented sandstone samples

Sample category	Name (Garticle grade)	Diameter (mm)	Height (mm)	Mean size (mm)	Density (g·cm^{-3})	Water content (%)	Porosity (%)
Single grain size	A (II)	49.87	100.05	0.1625	2.21	28.32	36.53
	B (III)	49.21	100.12	0.375	2.27	28.32	36.53
	C (IV)	49.26	100.09	0.75	2.26	28.32	36.51
	D (V)	49.51	100.12	1.5	2.24	28.32	36.50

	E (VI)	49.34	100.25	3.5	2.25	28.32	36.50
Two group grain size	F (I+II)	49.58	100.18	0.1	2.23	28.32	36.49
	G (II+III)	49.68	100.08	0.26875	2.23	28.32	36.54
	H (III+IV)	49.87	100.15	0.5625	2.21	28.32	36.50
	I (IV+V)	49.91	100.07	1.125	2.21	28.32	36.51
	J (V+VI)	49.25	100.15	2.5	2.26	28.32	36.52
Naturally gradation	K (I~VI)	49.71	100.09	—	2.22	28.32	36.49
	L (I~VI)	49.52	100.16	—	2.24	28.32	36.50

Sieving

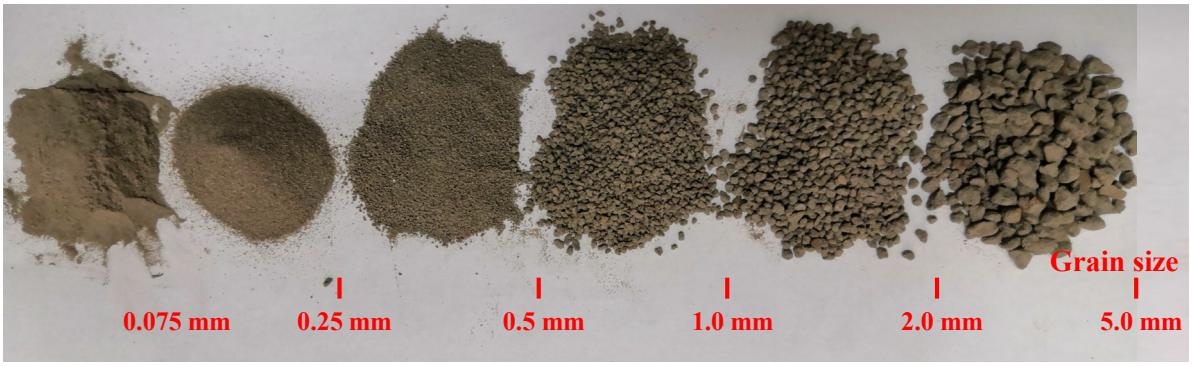

Preparation

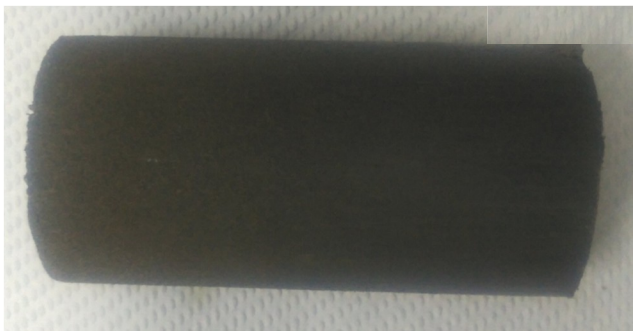

Figure 3 Process of sample preparation

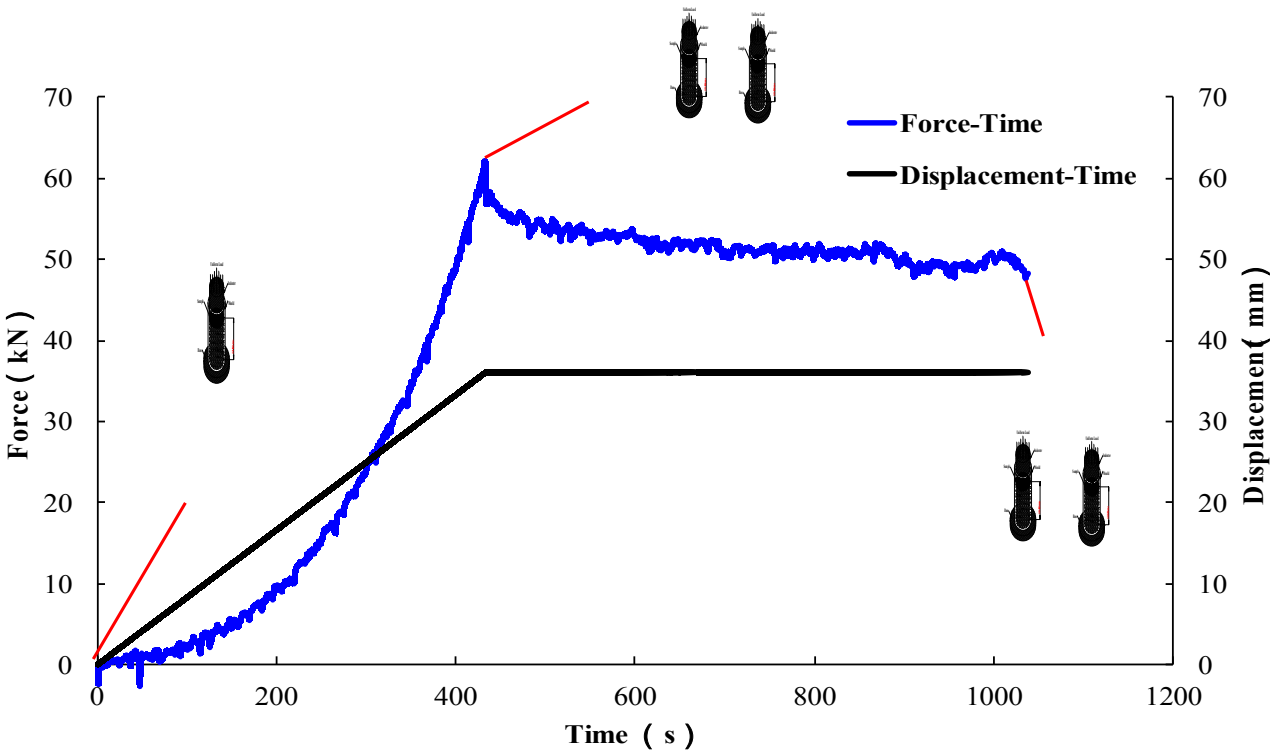

Figure 4 Sample preparation process and preparation curve

2.5 Testing methods of permeability

The permeability tests are performed using the high hydrostatic stress core seepage setup, which is developed in Institute of Rock and Soil Mechanics, Chinese Academy of Sciences. The system consists of four major components: core holder system, hydrostatic stress loading system, pore pressure loading system and data acquisition system. The maximum pore pressure 45 MPa can be applied with the accuracy of 0.01 MPa, and the maximum hydrostatic stress 60 MPa with the accuracy of 0.01MPa can be loaded. Both can be applied in two modes, i.e., the constant stress loading and constant flow loading. The schematic of the test system is shown in Figure 5.

Saturated uncemented sandstone samples are placed in the high hydrostatic stress core seepage setup. Two seepage plates with full circular diversion trench (Figure 6) are placed at the ends of the prepared sample, where the sterilized distilled water flows along the radial guide grooves and seepages in the axial direction through the holes in guide grooves. A hydrostatic stress is loaded to in-situ stress equal to 12.50 MPa, and remains to constant. After the deformation of sample is stable, the permeability of samples is measured under different flow rate condition. At the beginning of the test, the applied flow rate is 0.10 ml/min. The pore pressure is recorded when the outlet of the high hydrostatic stress core seepage setup evenly drops and the pore pressure is stable. Then, the flow rate is increased step by step until the failure

of prepared sample. The schematic diagram of permeability measurement is shown in Figure 6. The applied mode of the flow rate is as follows:

$$0.1\ \text{ml/min} \xrightarrow{+0.1} 1.0\ \text{ml/min} \xrightarrow{+0.25} 6.0\ \text{ml/min} \xrightarrow{+0.5} 15.0\ \text{ml/min}$$

The Darcy's law (i.e., Eq. 7), is adopted to calculate the absolute permeability based on the relationship between hydraulic gradient and flow rate, where the flow rate can be calculated by equation (6).

$$v = \frac{14.4Q}{A\varphi} \tag{6}$$

where v is the flow rate, m/d; Q is the flow, ml/min; A is the cross-sectional area of the prepared samples, cm^2; φ is the porosity of the prepared samples, %.

$$J = \frac{\mu}{K} v \tag{7}$$

where K is the absolute permeability of the prepared sample, which can be calculated based on the *J*-*v* curve. □m^2; μ is the dynamic viscosity coefficient, 1.005×10^{-3} Pa•s; J is the pore pressure gradient, MPa/m.

In addition, the apparent permeability (AP) of the sample can reflect its grain migration and pore structure reconstruction (Wang et al., 2019b; Sheng et al., 2019), as shown in equation (8).

$$K_{ap} = \frac{\mu}{J_{rt}} v \tag{8}$$

where K_{ap} is the apparent permeability of the prepared sample, which varies with grain migration or pore structure reconstruction, □m^2; J_{rt} is the pore pressure gradient in real-time, MPa/m.

Figure 5 Schematic diagram of the test system

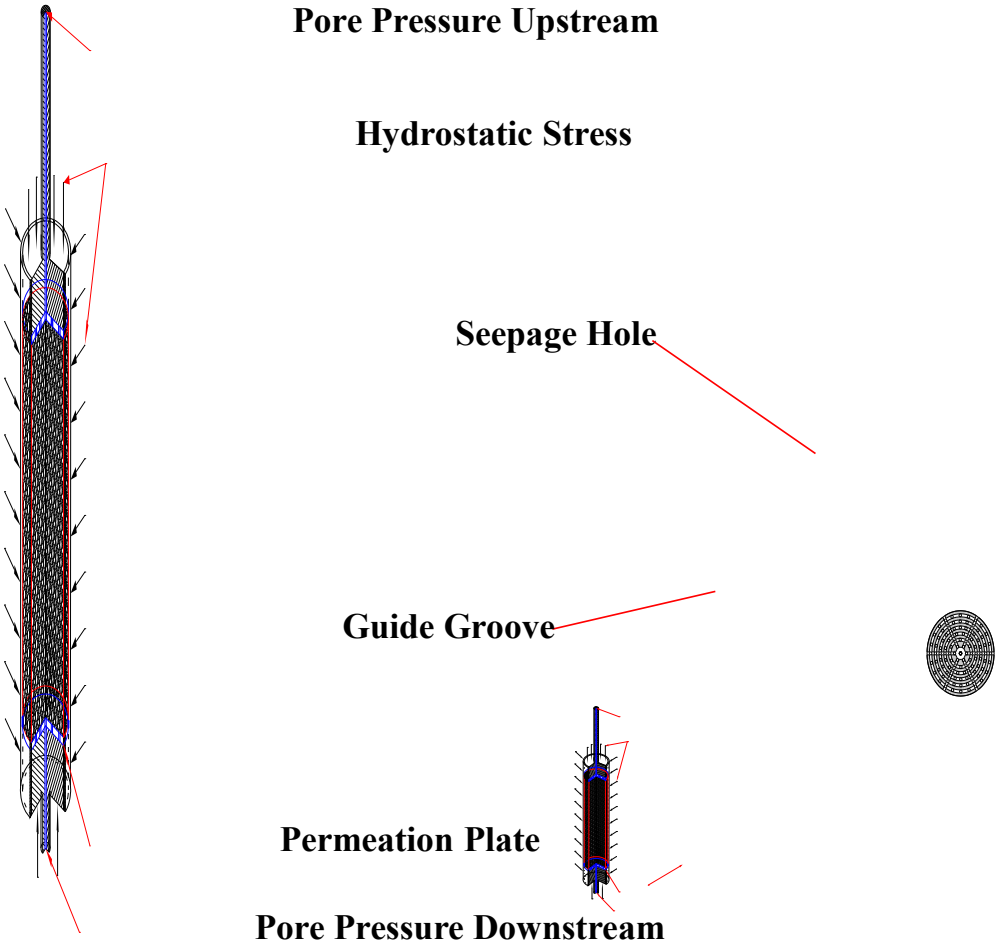

Figure 6 Schematic diagram of permeability measurement

3 Results

This work mainly focuses on the coupling effect of in-situ stress and grain-migration on clogging during groundwater recharge for uncemented sandstone reservoir, and the effect of grain composition and flow rate on the transportation properties. Thus, the permeability tests of uncemented sandstones with different grain compositions (e.g. SGS, DGS and NG) under in-situ stress are carried out respectively.

3.1 Permeability characteristics of samples with SGS

The permeability characteristics of uncemented sandstones with SGS under in-situ stress is shown in Figure 7. The results showed that there is a linear relationship between the flow rate and the pore pressure difference, presenting an obvious Darcy seepage characteristic. The absolute permeability can be calculated by equation (6), and it has a decline trend with the increase of mean grain size (Figure 8). In addition, the apparent permeability of uncemented sandstones with SGS tends to be constant with the increased flow rate, and even exhibition with a transition from increased to stable for sample A with the grain size of 0.075mm~0.25mm. However, it should be noted that the pore pressure at failure varies from 6.33 MPa to 7.31 MPa for all samples.

The absolute permeability of sample A is significantly greater than that of other samples. The apparent permeability exhibits a transition from increased to stable with the flow rate. The flow rate in the sample A is much larger than other samples at failure state. The grain size distribution of the whole samples after the permeability test is calculated (Figure 9). The results show that the abnormal grains appear in the sample due to the original grains are crushed or even broken into fine grains under in-situ stress (Hall and Harrisberger, 1970; Feda, 2002; Zivar et al., 2019). The sample A has the lowest content (only with 2.13 %) of abnormal grains compared with other samples. Therefore, its pore structure has a low-probability of being clogged. The absolute permeability of sample A is significantly greater than that of other samples, and a larger flow rate of fluid can be passed through its pore structure. Furthermore, the result shows that the fine grains can roll and slide under the action of current scouring (Hall and Harrisberger, 1970), which means that the fine grains in the pore structure can migrate, and then dredge the seepage channel, especially for sample A with a fine grain content of only 2.13 %. Thus, the apparent permeability of sample A gradually increases until the end of grain migration. However, the abnormal grain cannot migrate through the pore structure due to the high content and large size in other samples. It can be proven in two ways. On the one hand, the migration of abnormal grains will cause a change in the apparent permeability (Baveye et al., 1998; Ozgurel and Vipulanandan, 2005), whilst there is no significant change in the apparent permeability in other samples. On the other hand, the migration of abnormal grains will cause a nonuniform distribution of fine grain in different parts of the samples, whilst the content of fine grains at both ends of the samples is basically equal after the permeability test (Figure 16).

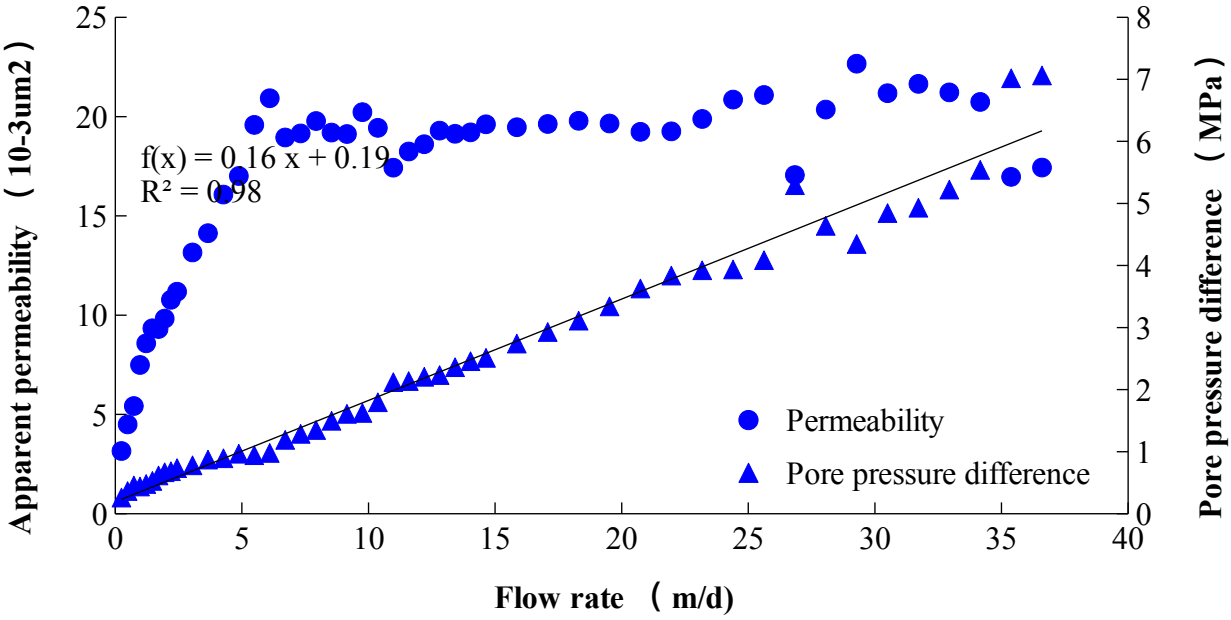

(a) Sample A (0.075 mm ~ 0.25 mm)

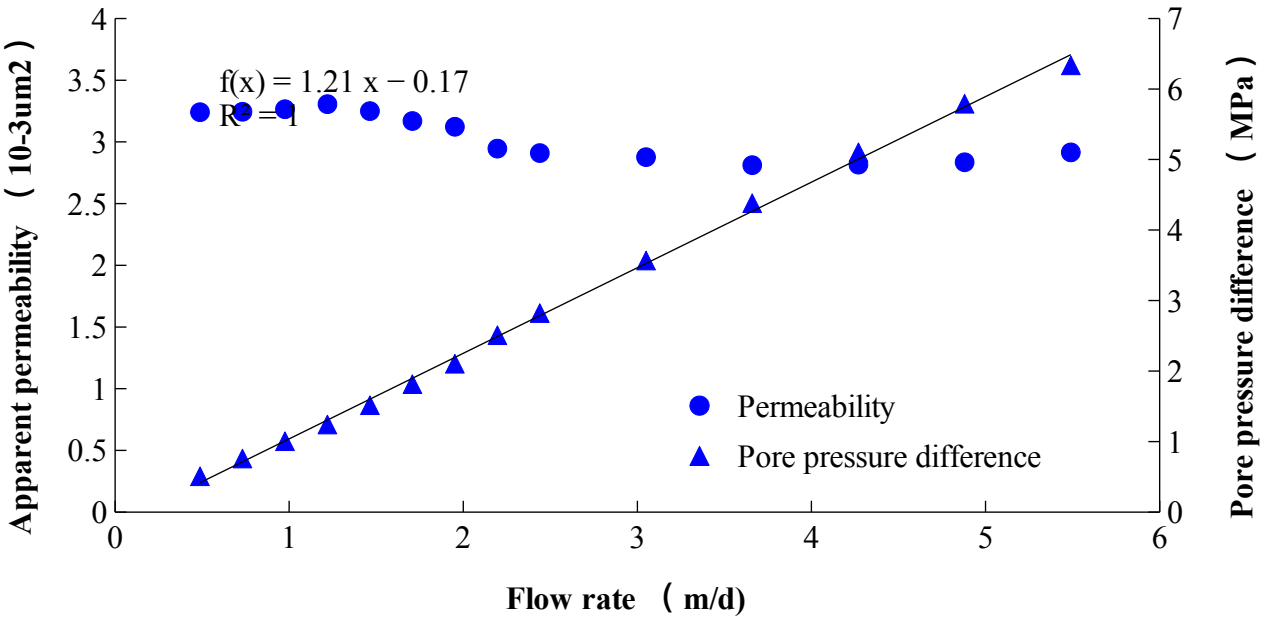

(b) Sample B (0.25 mm ~ 0.5 mm)

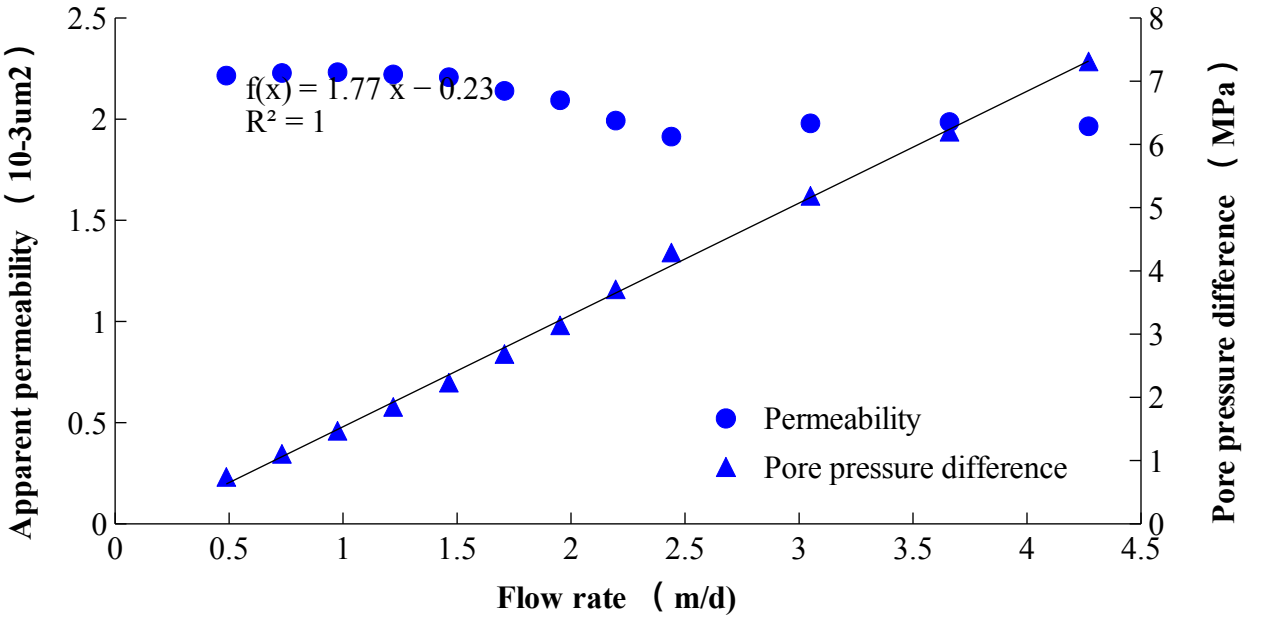

(c) Sample C (0.5 mm ~ 1.0 mm)

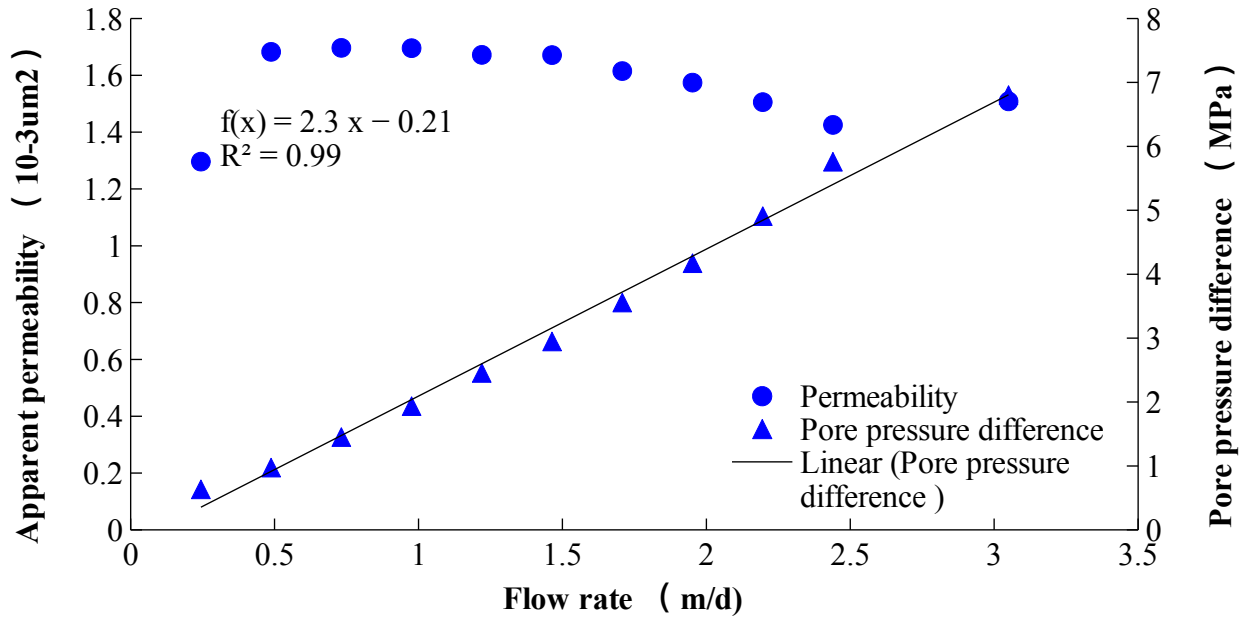

(d) Sample D (1.0 mm ~ 2.0 mm)

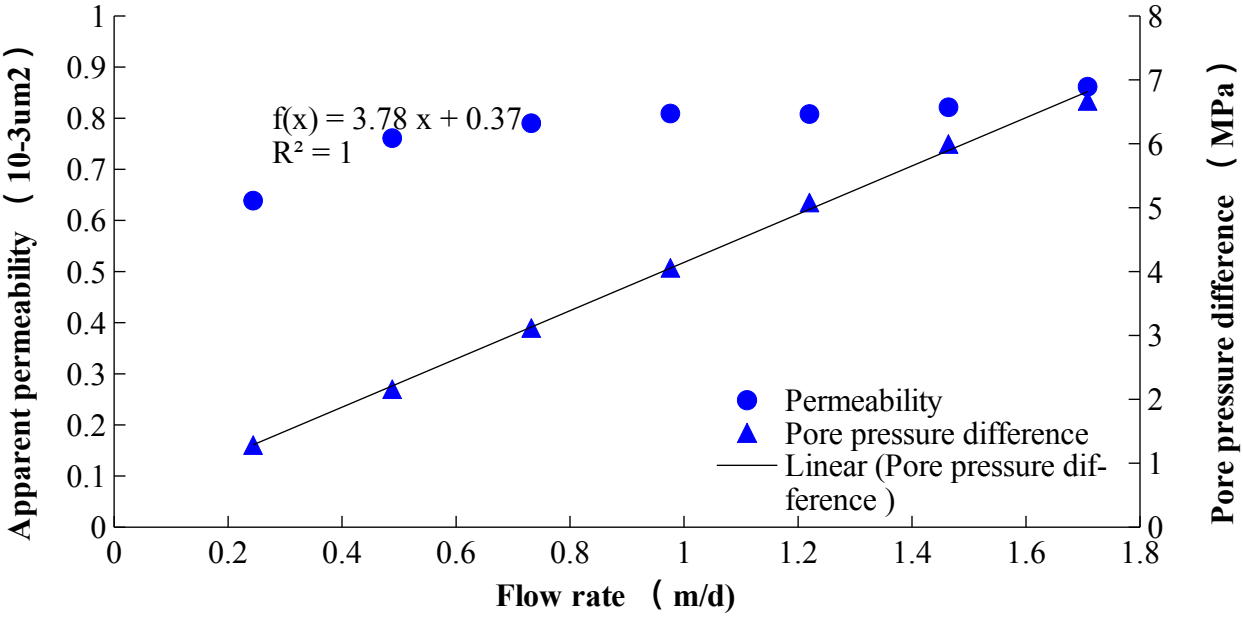

(e) Sample E (2.0 mm ~ 5.0 mm)

Figure 7 The permeability characteristics of uncemented sandstones with SGS

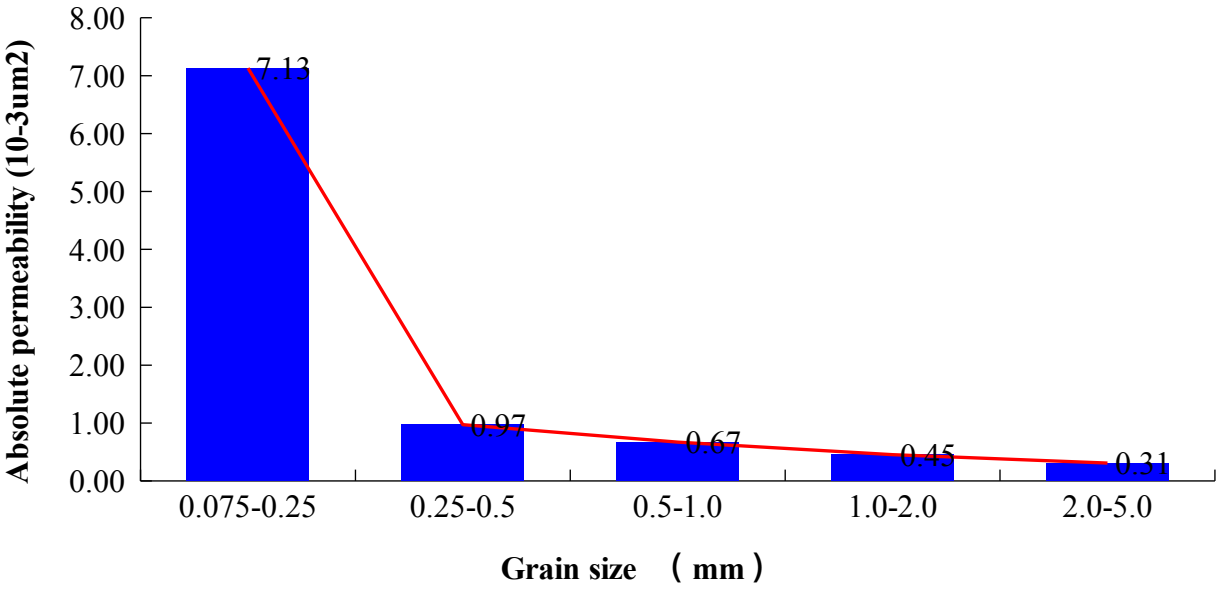

Figure 8 The relationship between absolute permeability and Grain size for the uncemented sandstones with SGS

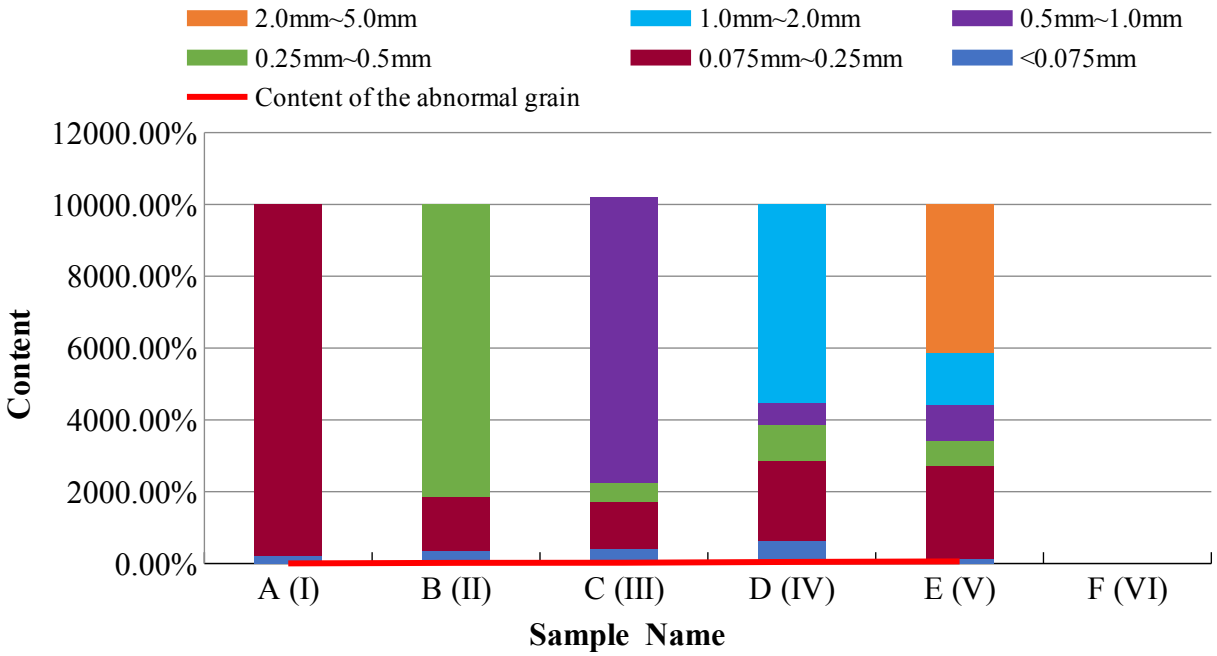

Figure 9 The grain size distribution of the sample after the permeability test for the uncemented sandstones with SGS

3.2 Permeability characteristics of samples with DGS

The permeability characteristics of uncemented sandstone with DGS under in-situ stress condition during the flow state is measured (Figure 10). The results show that there is a significant linear relationship between the flow rate and the pore pressure difference, which is

consistent with the Darcy seepage characteristics. Thus, its absolute permeability can be calculated by equation (6), and it gradually decreases with the increased mean grain size (Figure 11). Moreover, the apparent permeability of samples F and G experience a short period of stability at the initial stage, followed by a gradual decrease until the failure of samples. However, the samples H, I and J exhibit a different variation, where the apparent permeability skips a short period of stability and goes directly into the decrease stage, after which it gradually stabilizes. Nevertheless, the pore pressure does not change significantly when the samples are at failure, with a range from 6.53 MPa to 7.69 MPa.

However, it is interesting that the apparent permeability of samples F and G exhibit a different variation trend compared with that of samples H, I and J. For samples F and G, at the beginning of experiment the pore pressure does not reach the initial stress of fine grains (Richards Reddy, 2012; Van Beek et al., 2014; Vandenboer et al., 2019). Thus, the fine grains do not migrate and the apparent permeability is stable. Nevertheless, a large number of fine grains migrate and block the seepage channel with the increase in pore pressure, which causes a decrease in apparent permeability. Studies have shown that the critical initial stress of the grains is inversely proportional to grain size (Skempton et al., 1994; Wang and Qiu, 2017b; Huang et al., 2017b). Therefore, the pore pressure reaches the critical initial stress of grains at the beginning of experiments for samples H, I and J with larger size grain. The fine grains migrate along the space between the skeleton structures, and gradually deposit at the bottom of the sample, blocking the seepage channel, which leads to a gradual decrease in apparent permeability. However, as the experiment progresses, the grain migration gradually stabilizes or stops, and then the apparent permeability tends to be stable. This could be proved by the grain size analysis results for samples with DGS, after permeability experiments, which will be discussed in Sec. 4.2.

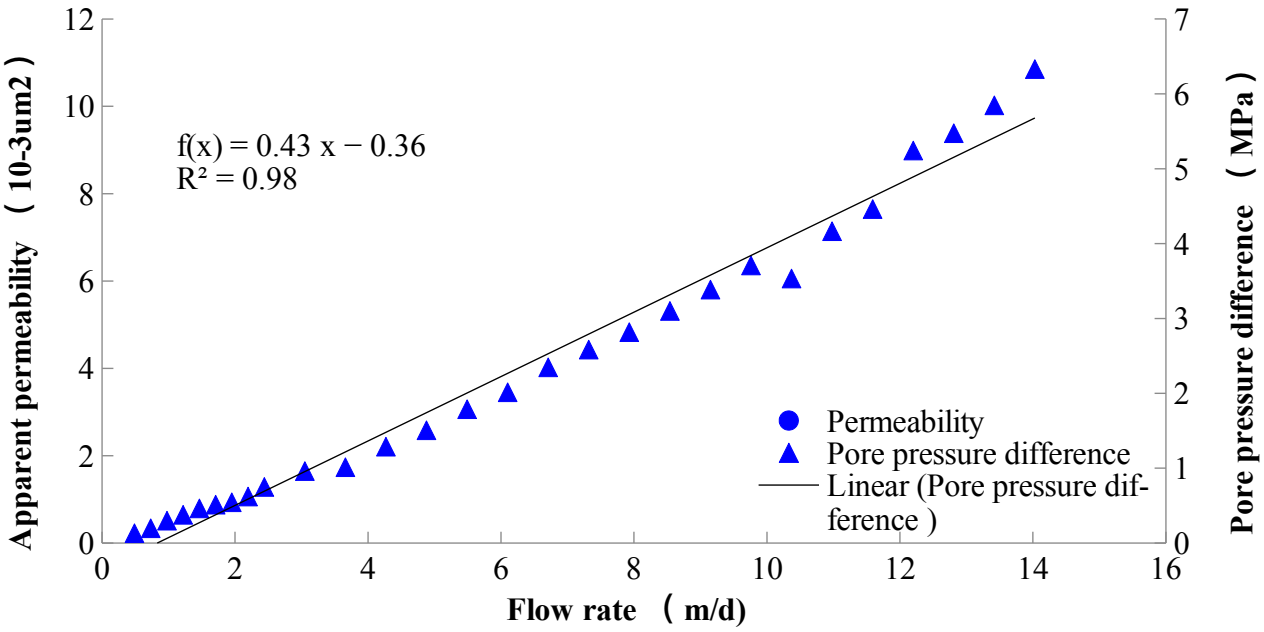

(a) Sample F (< 0.075 mm + 0.075 mm ~ 0.25 mm)

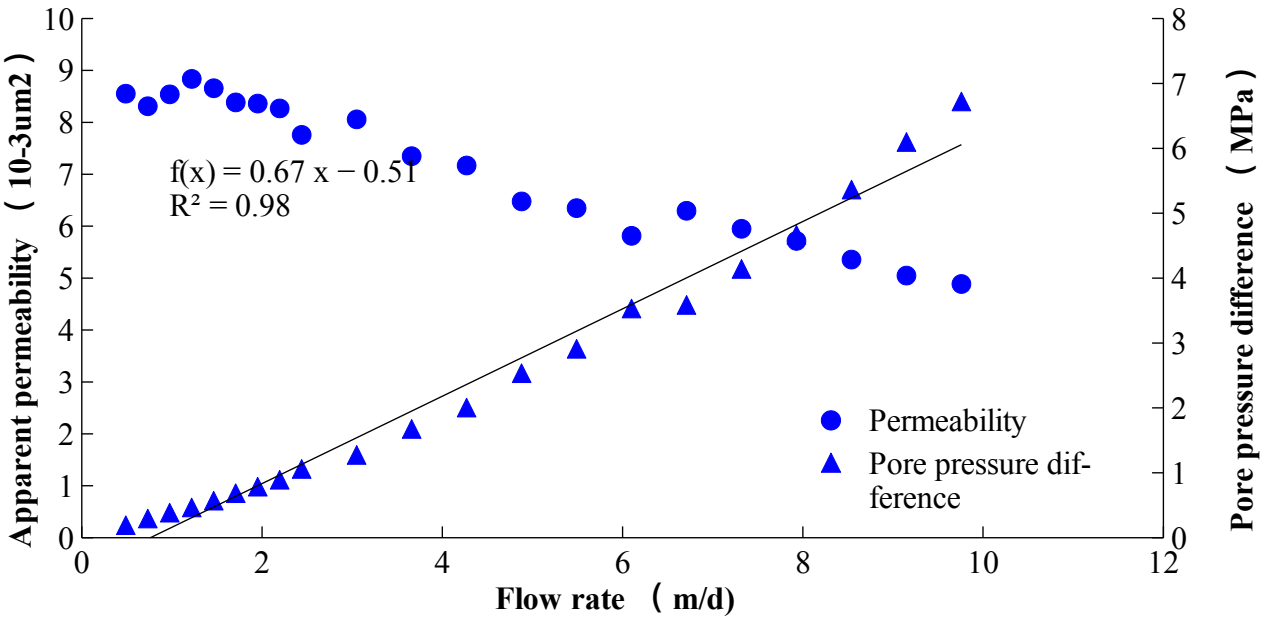

(b) Sample G (0.075 mm ~ 0.25 mm + 0.25 mm ~ 0.5 mm)

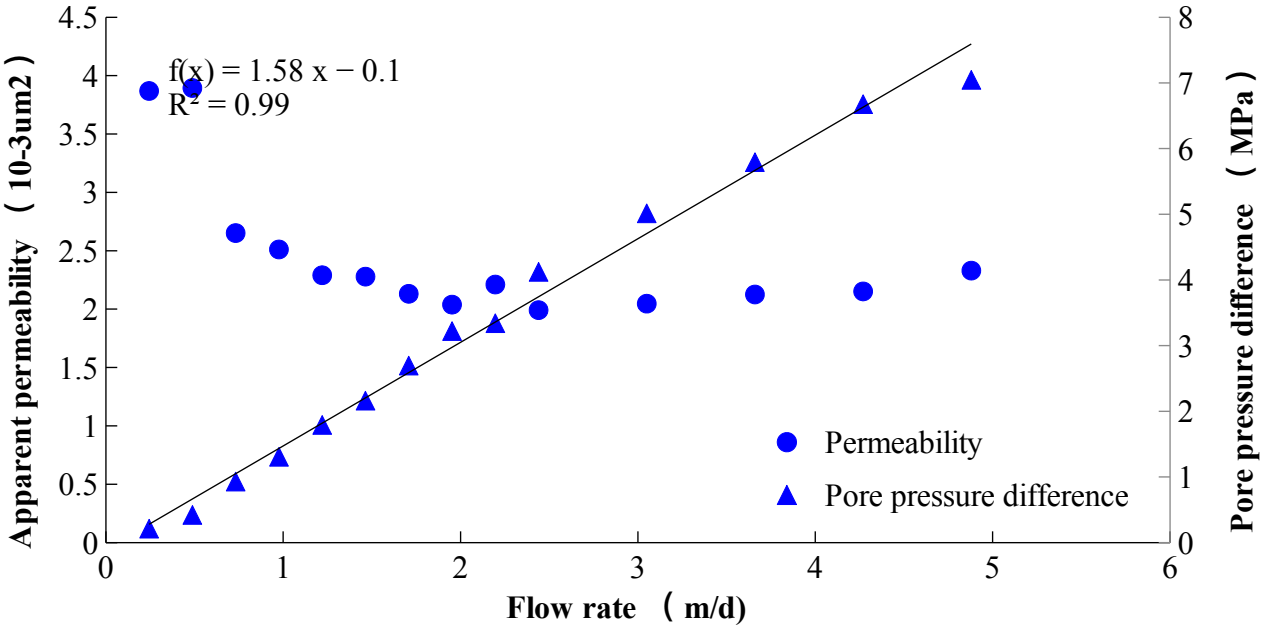

(c) Sample H (0.25 mm ~ 0.5 mm + 0.5 mm ~ 1.0 mm)

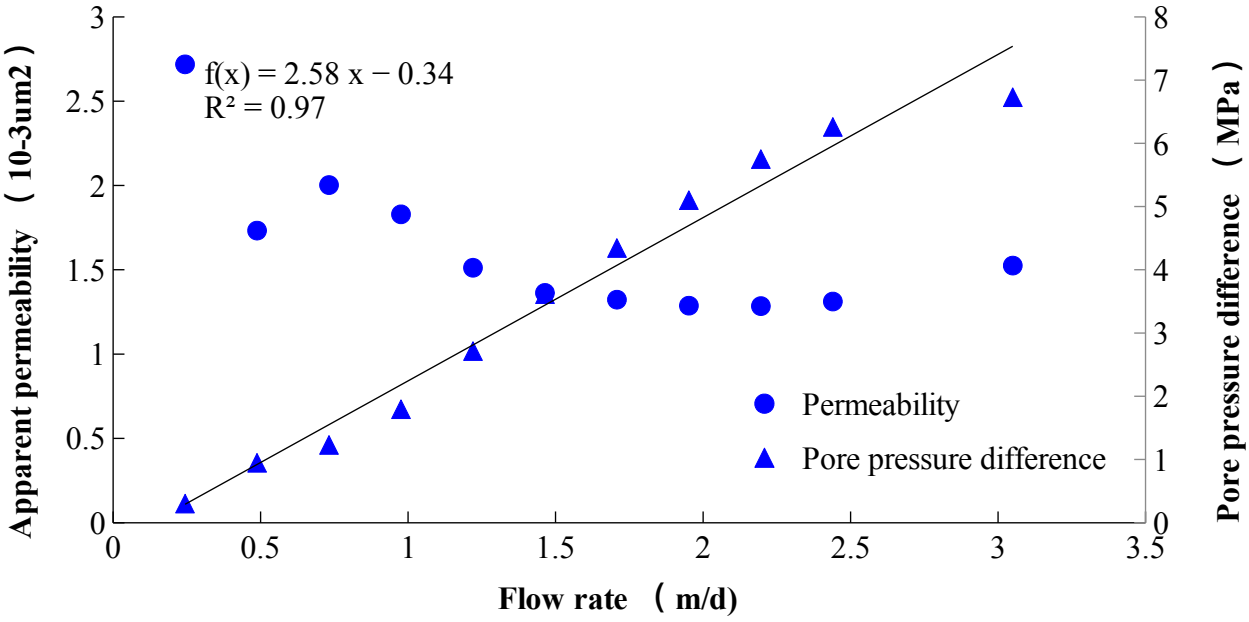

(d) Sample I (0.5 mm ~ 1.0mm + 1.0 mm ~ 2.0mm)

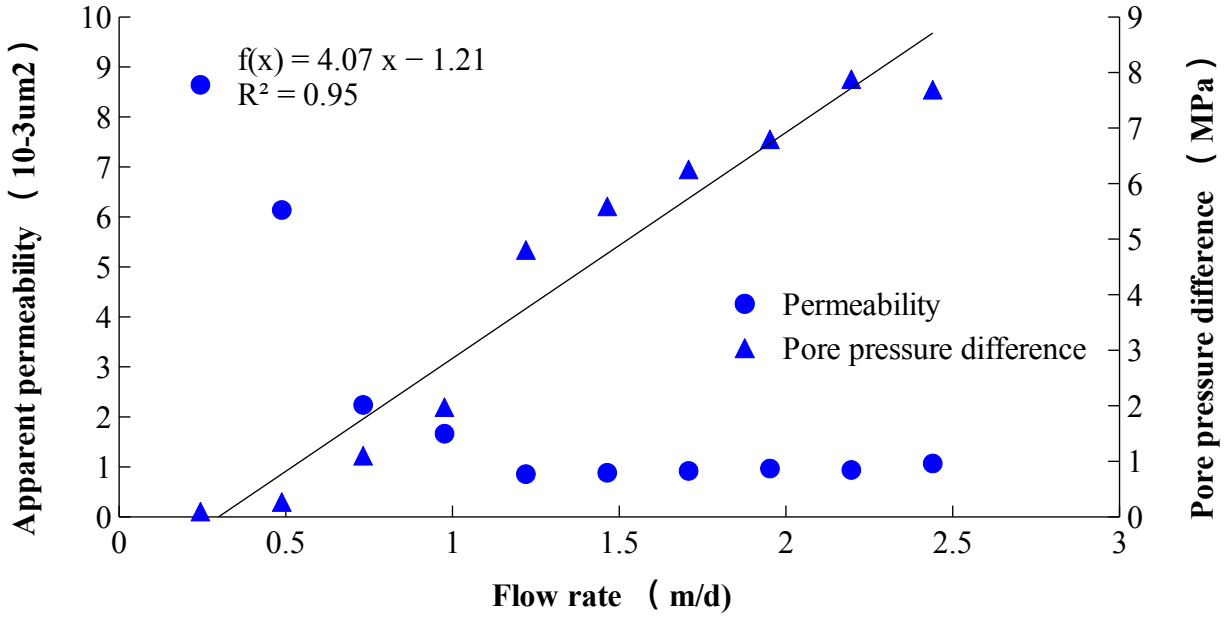

(d) Sample J (1.0 mm ~ 2.0mm + 2.0 mm ~ 5.0mm)

Figure 10 The permeability characteristics of uncemented sandstones with DGS

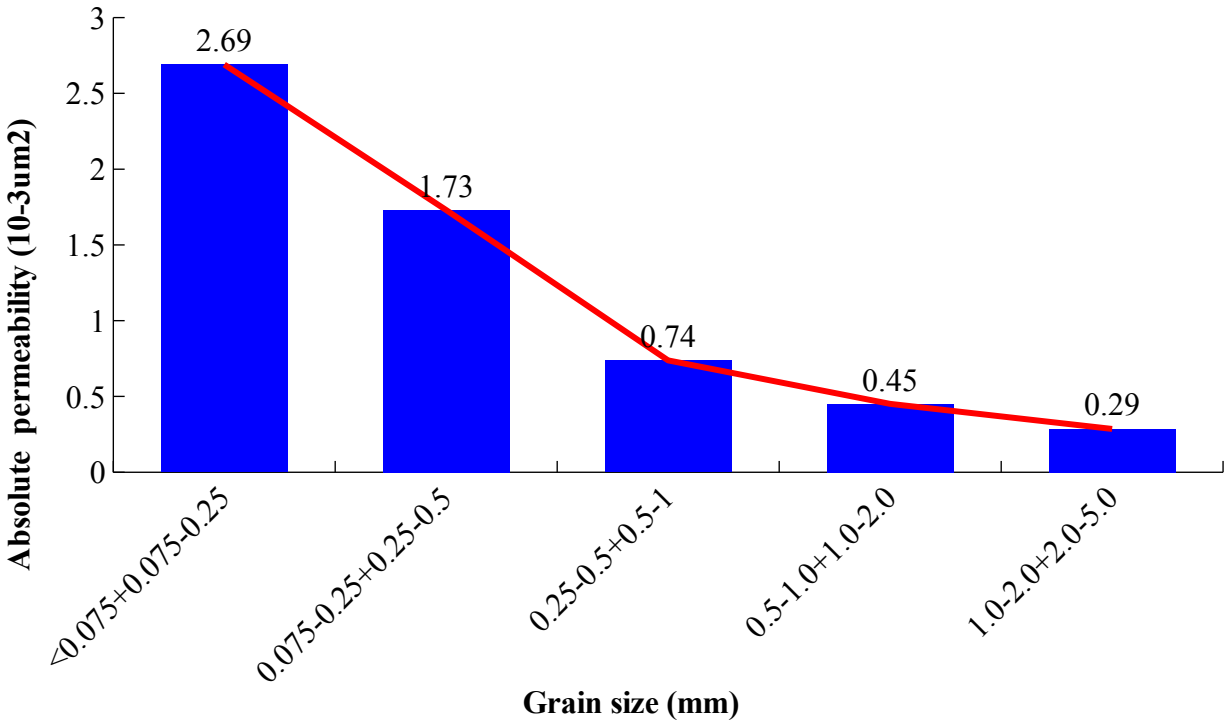

Figure 11 The variation in absolute permeability with grain size for the uncemented sandstones with DGS

3.3 Permeability characteristics of samples with naturally gradation

The permeability measurement of uncemented sandstones with NG with flow rate under in-situ stress are carried out (Figure 12). The results show that a linear relationship between the flow rate and the pore pressure difference is suitable for samples K and L. The absolute permeability can be calculated by equation (6). Meanwhile, the uncemented sandstones with NG, samples K and L, whose apparent permeability have dropped rapidly, and soon it stabilizes at around 1.0×10^{-3} um^2. In addition, the pore pressure of the sample at failure state are 6.5 MPa and 7.3 MPa for samples K and L, respectively.

However, it is interesting that the flow rate at which the permeability of samples K and L reach a stability are basically consistent with samples H, I and J, with a range from 1.22 m/d to 2.44 m/d, whilst a larger flow rate of fluid can flow through the samples K and L in the range of 24.4 m/d and 29.28 m/d. It is explained that the structure of the uncemented sandstone with NG is more stable than that of samples with DGS. The similar findings are also drawn by Hall and Harrisberger (1970), Chen et al. (2017) and Yang et al. (2019).

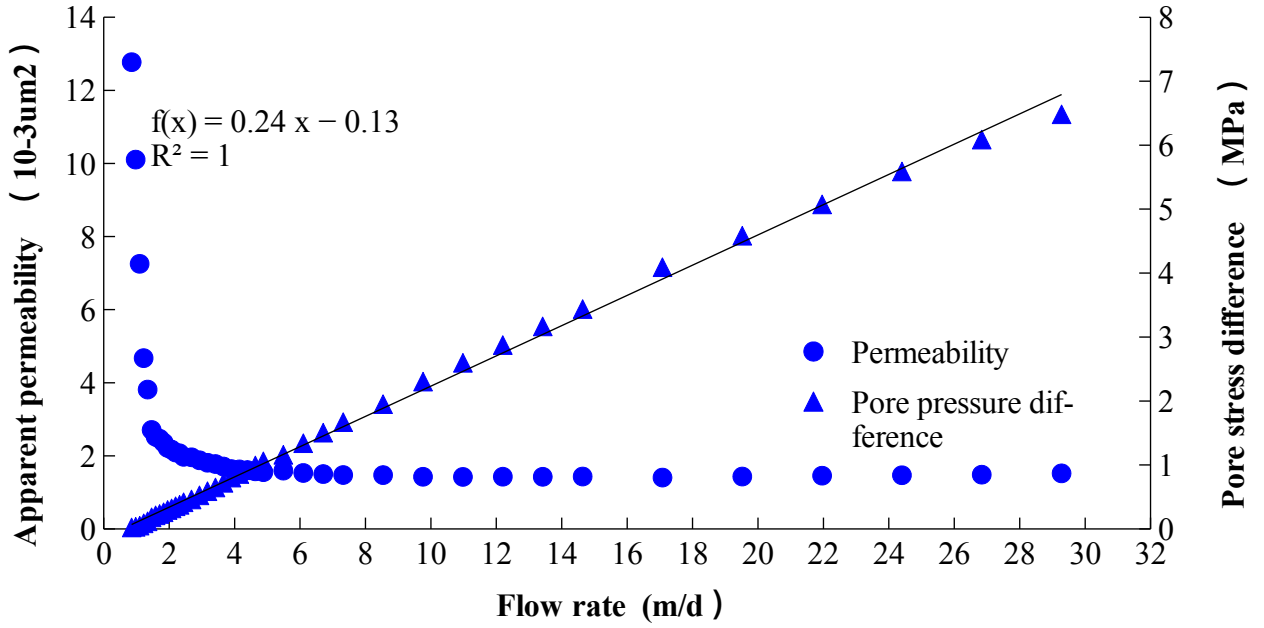

(a) L (Naturally Gradation)

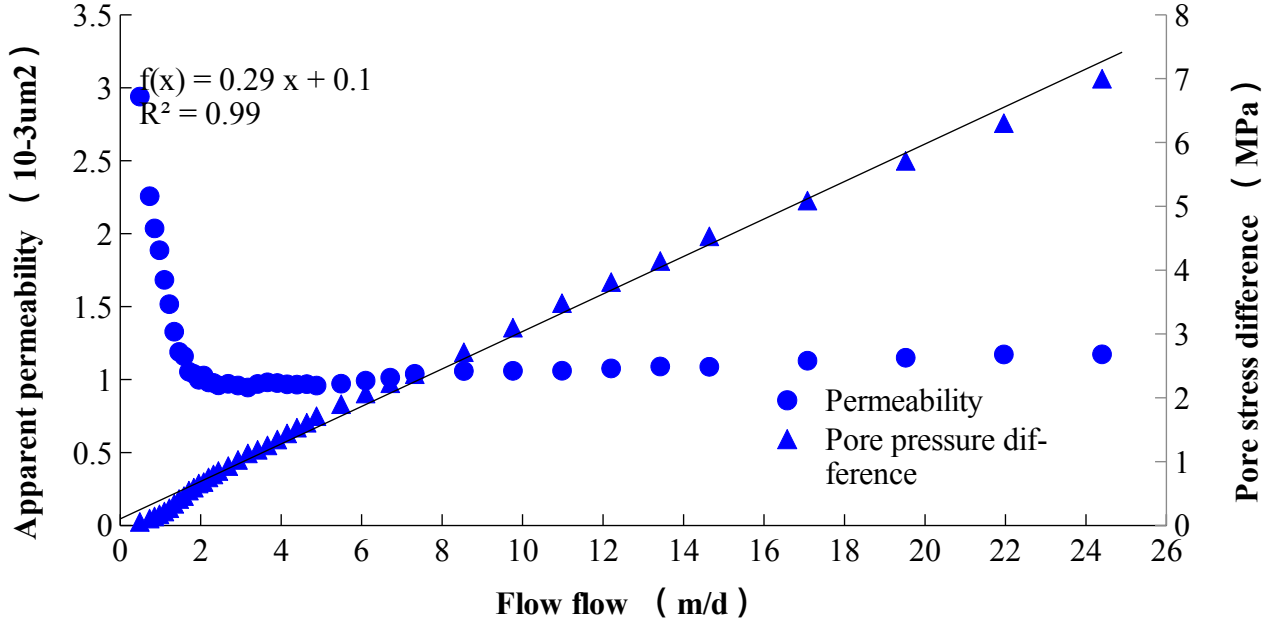

(a) M (Naturally Gradation)

Figure 12 The permeability characteristics of uncemented sandstones with NG

3.4 Variations in absolute permeability and pore pressure at failure

From the above test results, the absolute permeability decreases with the increased grain size, whilst the pore pressure increases with the increase of flow rate and tend to a constant equal to 1/2 of applied hydrostatic stress. Therefore, the mean grain size is used as a variable to analyze its absolute permeability and pore pressure at failure for samples with SGS and DGS (Figure 13), and the results are shown in Table 4.

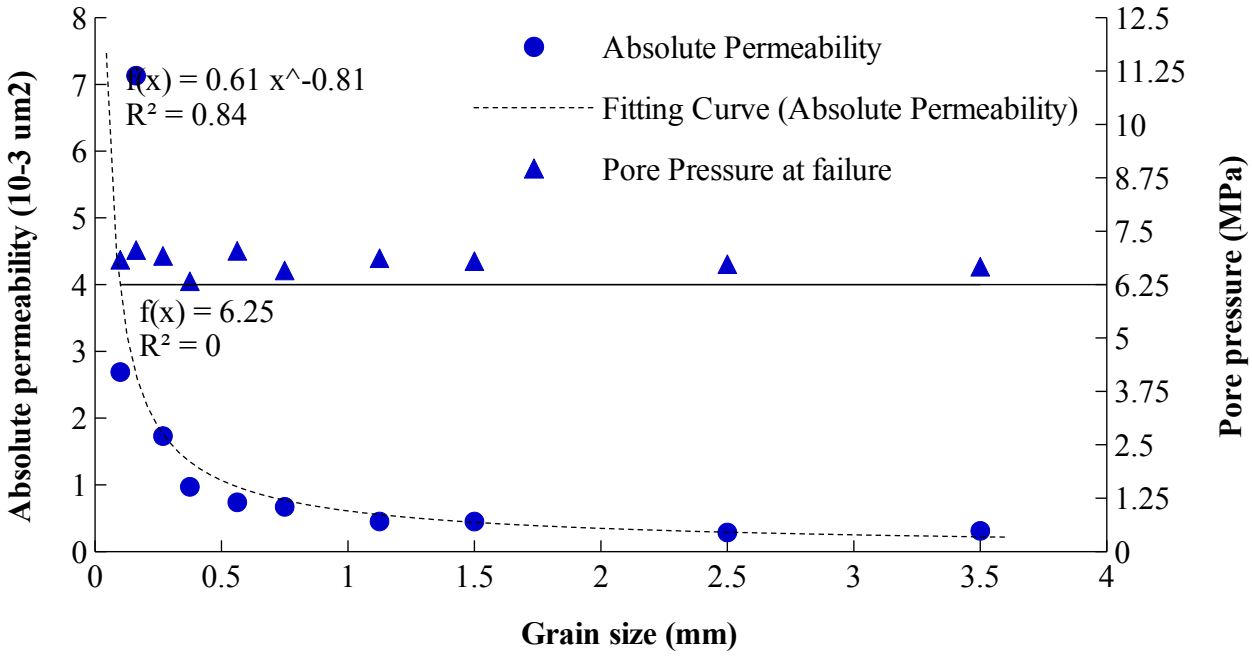

Figure 13 Variations in absolute permeability and pore pressure with grain size

It is interesting to find that the permeability and grain size for the uncemented sandstone presents a negative correlation, which is totally different from that of many previous studies (Krumbein and Monk, 1943; Chilingar, 1964; Masch and Denny, 1966; Chapuis, 2004; Ozgurel and Vipulanandan, 2005; AlHomadhi, 2014; Wang et al., 2019a; Huang et al., 2019). The main reason for this phenomenon is that the confining stress is not considered or the applied confining stress is too small in many previous experiments, which are greatly different from the in-situ stress conditions of the geothermal reservoirs in the fields, especially for the extraction of higher temperature groundwater (Templeton et al., 2014; Nian and Cheng, 2018a). The original grains are crushed or even broken into fine grains under in-situ stress, and then blocking the seepage channel. Furthermore, the content of fine grains increases with the increased grain size (Figure 9), thus, the permeability decreases with the increased grain size under in-situ stress. In addition, the pore pressure at failure tends to a constant equal to 1/2 of the applied hydrostatic stress for all the samples. This indicates in-situ stress and pore pressure are key factors controlling the failure of uncemented sandstone, but excluding grain composition.

4 Discussion

4.1 Analysis of high pore pressure gradient

It should be pointed out that the pore pressure gradient as high as 633–731 kPa/cm occurs when the samples are at failure under in-situ stress equal to 12.50 MPa, which are much higher than the critical hydraulic gradient of cohesive or gravel soil in previous studies (Dixon et al., 1992; Wang et al., 2014; Israr and Indraratna, 2019). This may be explained in two ways (Yang et al,. 2019). Firstly, no confining stress is considered or the applied confining stress is quite small in previous studies, causing a low critical hydraulic gradient for the cohesive or gravel soil. However, the results obtained by Chang & Zhang, (2013) and Xiong et al. (2018b) show that the critical hydraulic gradient of the samples significantly increase after a confining stress is applied.

Secondly, the clogging caused by physical, chemical and biological factors is the inevitable problem during groundwater recharge in the field (Pavelic et al., 1998; Rehg et al., 2005; Katarzyna, 2006), which causes a rapid rise of recharge pressure and a low recharge efficiency. This phenomenon is also observed during groundwater recharge of GWHP systems in Jianghan Oilfield. Therefore, measures such as well washing and acidification have to be taken to reduce the recharge pressure in field (Su et al., 2018). Meanwhile, this further demonstrates that the experiments performed can simulate the recharge clogging in the field, from which the clogging mechanisms can be revealed by laboratory experiments, and then some suggestions about the operation of GWHP systems can be summarized.

4.2 Clogging mechanism of uncemented sandstone under hydrostatic stress

The pore pressure gradually increases with the increased flow rate until the sample are at failure, as high as 6.33–7.31 MPa, and the apparent permeability decreases and gradually stabilizes for the samples with NG and DGS. The essential reason is that the recharge clogging caused by grain migration. Firstly, the original grains are crushed even broken into the fine grain under in-situ stress. Then, the fine grains originally filled or secondary crushed are migrated along the space between the skeleton structures and gradually deposite at the lower parts of the sample under seepage compression. This could be gained from the grain size distribution of different parts of samples with DGS (Figure 14). It shows that the abnormal grains appear in sample due to the crushing effect of in-situ stress, and the content of fine grains in Part II is significantly higher than that of Part I, where the fine grains in Figure 14 mean that all grains with a diameter smaller than that of the maximum constituent grain. It strongly proves that the fine grains migrate from Part I to Part II during groundwater recharge for uncemented sandstones with DGS. Meanwhile, the migrated grains block seepage channel, resulting in the increase in pore pressure and the decrease in apparent permeability. Moreover, the grain migration creates a space between the skeletal structure in the Part I of sample, and the resistance to deformation is weakened. Furthermore, the fine grains between the skeleton structure in Part II of sample are more denser, and the resistance to deformation is strengthened. Under high pore pressure and in-situ stress, the skeleton grains in Part I are deformed and moved, resulting in a diameter shrinkage. Therefore, the diameter shrinkage occurs in the upper part for the sample with NG and DGS. A comparison of the grain migration and the failure mode I in the conceptual model is based on the analysis of grain size (Figure 15).

Moreover, the pore pressure gradually increases linearly with the increase of flow rate, and the apparent permeability tends to be constant, and even exhibition with a transition from increased to stable, which indicates no grain migrates for the uncemented sandstones with SGS. This can also be proven by the result of grain size distribution in different parts of sample (Figure 16). The content of fine grains in the middle of sample is significantly higher than that in both ends of the sample, and the fine grain content at both ends of sample is basically equal, where the fine grains have a diameter smaller than the size of maximum constituent grains. However, a large number of fine grains appear in the sample due to the original grain are crushed even broken into fine grain under in-situ stress (Figure 9), especially for the skeleton grains with larger size. Thus, the skeleton structure will be reconstructed with a diameter shrinkage under the high pore pressure and in-situ stress, resulting in the decrease in absolute permeability with grain size. However, there is only a significant diameter shrinkage in the middle of the sample due to boundary conditions when two steel seepage plates are placed at the ends of the sample. A

comparison of the grain migration and the failure mode II in the conceptual model is based on the analysis of grain size (Figure 17).

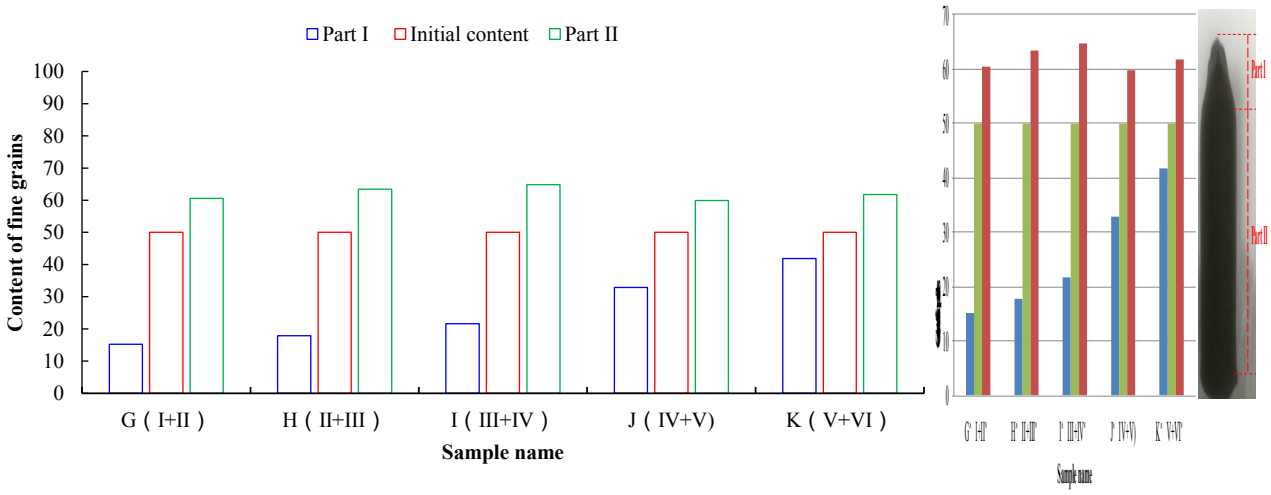

Figure 14 The content of fine grains of different parts for the uncemented sandstones with DGS

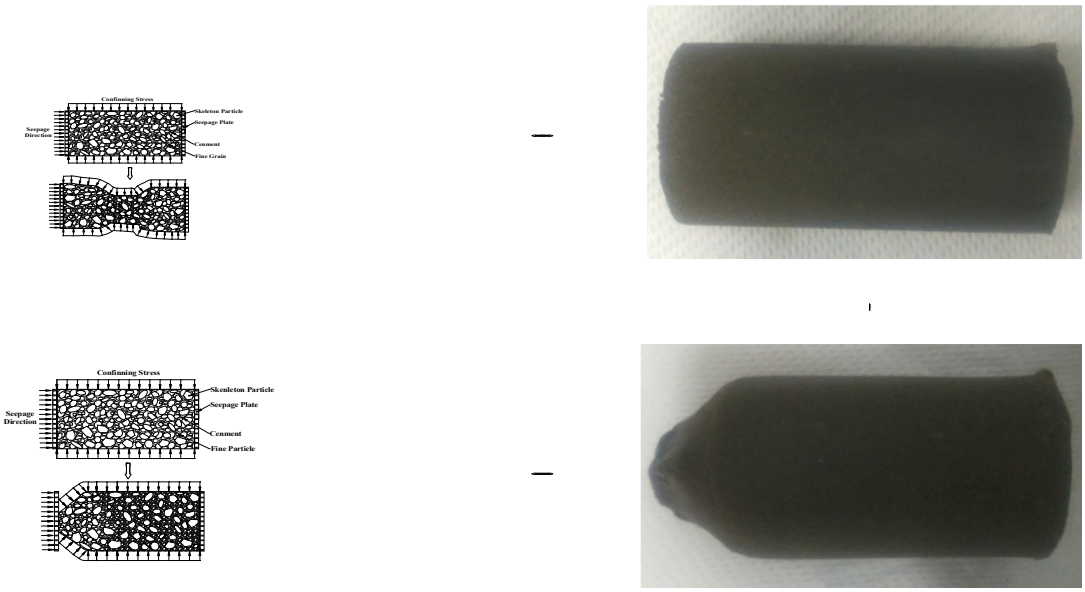

Figure 15 Comparison diagram of the grain migration and the failure mode I in the conceptual model

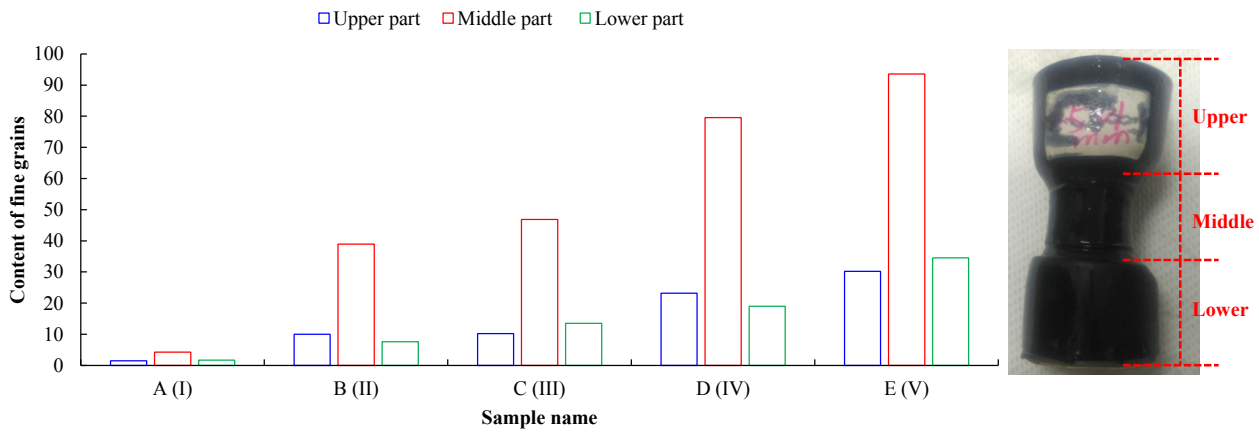

Figure 16 The content of fine grains of different parts for the uncemented sandstones with SGS

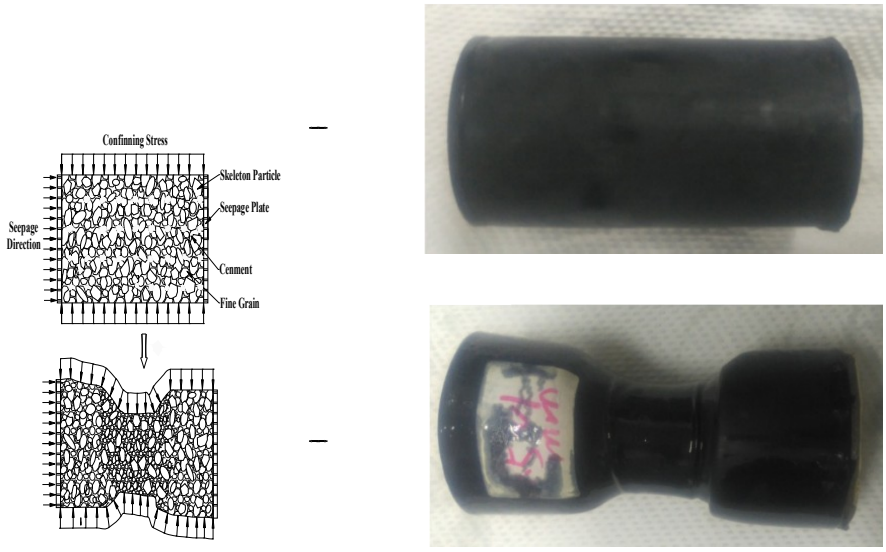

Figure 17 Comparison diagram of the grain migration and the failure mode II in the conceptual model

4.3 Suggestions for practical engineering

Furthermore, some suggestions could be provided for the utilization of geothermal energy for GWHP, especially for the deep hydrothermal reservoir with poor cementation. Firstly, the clogging problem caused by the grain migration under in-situ stress during groudwater recharge should be paid enough attention. This is an important reason of the decline in recharge efficiency for the uncemented sandstones reservoir, thus, some measures such as the sand filter and the cementing agent should be taken to weaken/prevent grain migration. Secondly, it is necessary to monitor the changes in geostress and recharge pressure during groundwater recharge, them of which are critical factors in controlling the stability of uncemented sandstones reservoir. In necessity, applicable measures could be taken to reduce the recharge pressure to ensure that the recharge well can be effectively used for a long time. Finally, the large-flow recharge is not recommended during groundwater recharge in field, which causes a rapid rise in recharge

pressure, accelerates the process of grain migration and clogging, and causes the decrease in recharge efficiency. Seriously, the formation deformation or subsidence may be occurred duo to grain migration in some cases.

5 Conclusions

In this work, three groups of samples with different grain compositions such as SGS, DGS and NG are prepared, using uncemented sandstone extracted from the target formation of hydrothermal engineering in Jianghan Oilfield, investigating the mechanisms of clogging caused by grain migration during groundwater recharge and the effect of grain composition and flow rate on the transportation properties. The conclusions can be drawn as follows:

(1) The clogging caused by the coupling effect of in-situ stress and grain-migration during groundwater recharge for uncemented sandstone. Firstly, the original grain are crushed even broken into fine grains under in-situ stress. Then, the fine grains originally filled or secondary crushed migrate along the space between the skeleton structure and gradually deposit at the bottom of sample for uncemented sandstone with DGS and NG, resulting in the increase in pore pressure and the decrease in apparent permeability. This has a good agreement with the observations during groundwater recharge of GWHP systems in Jianghan Oilfield. However, no obvious grain migration in the sample with SGS, whilst a large number of fine grains are observed in sample due to the compaction of in-situ stress, especially for the skeleton grains with larger size. Thus, the skeleton structure is reconstructed, resulting in the decrease in absolute permeability with grain size.

(2) The grain composition and flow rate have an obvious influence on the transportation properties. The Darcy seepage characteristics are exhibited for all samples. Apparent permeability exhibits different variation duo to the differences in grain composition, whilst the absolute permeability decreases with the increased grain size due to the compaction effect or/and the grain migration. Furthermore, the pore pressure increases with flow rate and tend to a constant equal to 1/2 of applied hydrostatic stress at failure. This indicates in-situ stress and pore pressure are key factors controlling the failure of uncemented sandstone, but excluding grain composition.

(3) Some suggestions could be provided for the utilization of hydrothermal geothermal energy for GWHP system, especially for the deep sandstone geothermal reservoir with poor cementation. Firstly, the grain migration under in-situ stress during groundwater recharge is an important reason of the decline in recharge efficiency, some necessary measures such as the sand filter and the cementing agent should be taken to weaken/prevent grain migration. Secondly, geostress and recharge pressure are critical factors in controlling the stability of uncemented sandstones reservoir, whose changes should be monitored in real time. Finally, in practical engineering, it is forbidden to use the large-flow recharge model to increase the recharge rate of groundwater, which will causes a rapid rise in recharge pressure, accelerates the process of grain migration and clogging.

Unfortunately, the studied samples are remoulded in this paper because the experimental material taken from the field is uncemented. Although it is prepared according to the density, water content and porosity of the sandstone geothermal reservoir, the characteristics of pore structure and the degree of consolidation are different. These disadvantage will be solved in the following works.

Acknowledgments and Data Availability Statement

- The data archiving is underway to a data repository of Mendeley Data with URL https://data.mendeley.com/
- The authors declare that there is no conflict of interest in the present study.
- The financial support by the National Key Research and Development Program of China (Grant Nos. 2018YFC0809600 and 2018YFC0809601), National Natural Science Foundation of China (Grant No. 51779252), and Major Technological Innovation Projects of Hubei, China (Grant No. 2017AAA128) for this work are gratefully acknowledged.

References

AlHomadhi, E. S. (2014). New correlations of permeability and porosity versus confining pressure, cementation, and grain size and new quantitatively correlation relates permeability to porosity. *American Journal of Geosciences*, 7(7), 2871–2879. https://doi.org/10.1007/s12517-013-0928-z

Barbier, E. (2002). Geothermal energy technology and current status: an overview. *Renewable & Sustainable Energy Reviews*, 6(1), 3-65. https://doi.org/10.1016/S1364-0321(02)00002-3

Barnaji, M. J., Pourafshary, P., & Rasaie, M. R. (2016). Visual investigation of the effects of clay minerals on enhancement of oil recovery by low salinity water flooding. *Fuel*, 184: 826-835. https://doi.org/110.1016/j.fuel.2016.07.076

Baveye, P. C., Vandevivere, P., Hoyle, B. L., Deleo, P. C., & De Lozada, D. S. (1998). Environmental Impact and Mechanisms of the Biological Clogging of Saturated Soils and Aquifer Materials. *Critical Reviews in Environmental Science and Technology*, 28(2), 123-191. https://doi.org/10.1080/10643389891254197

Bayer, P., Saner, D., Bolay, S., Rybach, L., & Blum, P. (2012). Greenhouse gas emission savings of ground source heat pump systems in Europe: A review. *Renewable & Sustainable Energy Reviews*, 16(2), 1256-1267. https://doi.org/10.1016/j.rser.2011.09.027

Bradford, S. A., Torkzaban, S., Leij, F. J., & Simunek, J. (2015). Equilibrium and kinetic models for colloid release under transient solution chemistry conditions. *Journal of Contaminant Hydrology*, 181, 141-152. https://doi.org/10.1016/j.jconhyd.2015.04.003

Bustos Medina, D. A., van den Berg, G. A., van Breukelen, B. M., Juhasz-Holterman, M., Stuyfzand, P. J. (2013). Iron-hydroxide clogging of public supply wells receiving artificial recharge: near-well and inwell hydrological and hydrochemical observations. *Hydrogeology Journal*, 21(7), 1393 – 1412. https://doi.org/10.1007/s10040-013-1005-0

Caulk, R., & Tomac, I. (2017). Reuse of abandoned oil and gas wells for geothermal energy production. *Renewable Energy*, 112, 388-397. https://doi.org/10.1016/j.renene.2017.05.042

Chang, D., & Zhang, L. M. (2013). Critical hydraulic gradients of internal erosion under complex stress states. *Journal of Geotechnical and Geoenvironmental Engineering*, 139(9), 1454-1467. https://doi.org/10.1061/(ASCE)GT.1943-5606.0000871

Chapelle, F, H. (1992). *Groundwater microbiology and geochemistry*, New York: NJ: John Wiley & Sons

Chapuis, R. P (2004). Predicting the saturated hydraulic conductivity of sand and gravel using effective diameter and void ratio. *Canadian Geotechnical Journal*, 41(5), 787–795.

Chen, J., Jiang, F. (2015). Designing multi-well layout for enhanced geothermal system to better exploit hot dry rock geothermal energy. Renewable Energy, 74: 37–48. https://doi.org/10.1139/t04-022

Chen, Z., Li, Y., Xie, Y., & Wang, X. (2017). In-situ Grain Migration and Plugging Mechanism in Uncemented sandstone and Sanding Management. *Chemistry and Technology of Fuels and Oils*, 53(5), 759-767. https://doi.org/10.1007/s10553-017-0858-7

Cheng, W., Li, T., Nian, Y., & Xie, K. (2014). An Analysis of Insulation of Abandoned Oil Wells Reused for Geothermal Power Generation. *Energy Procedia*, 61, 607-610. https://doi.org/10.1016/j.egypro.2014.11.1181

Cheng, W., Liu, J., Nian, Y., & Wang, C. (2016). Enhancing geothermal power generation from abandoned oil wells with thermal reservoirs. *Energy*, 109, 537-545. https://doi.org/10.1016/j.energy. 2016.05.009

Chilingar, G. V. (1964). Relationship Between Porosity, Permeability, and Grain-Size Distribution of Sands and Sandstones. *Developments in sedimentology*, 1, 71-75. https://doi.org/10.1016/S0070-4571(08)70469-2

Chu, T., Yang, Y., Lu, Y., Du, X., & Ye, X. (2019). Clogging process by suspended solids during groundwater artificial recharge: evidence from lab simulations and numerical modelling. *Hydrological Processes*, 33(25), 3226-3235. https://doi.org/10.1002/hyp.13553

Cui, X., Chen, C., Sun, S., Zhou, D., Ndayisenga, F., Huo, M., Zhu, S., Zhang, L., & Crittenden, J. C. (2018). Acceleration of saturated porous media clogging and silicon dissolution due to low concentrations of Al(III) in the recharge of reclaimed water. *Water Research*, 143, 136-145. https://doi.org/10.1016/j.watres.2018.06.043

Deo, O., Sumanasooriya, M. S., & Neithalath, N. (2010). Permeability Reduction in Pervious Concretes due to Clogging: Experiments and Modeling. *Journal of Materials in Civil Engineering,* 22(7), 741-751. https://doi.org/10.1061/(ASCE)MT.1943-5533.0000079

Dixon, D. A., Gray, M. N., & Hnatiw, D. (1992). Critical gradients and pressures in dense swelling clays. *Canadian Geotechnical Journal*, 29(6), 1113-1119. https://doi.org/10.1139/t92-129

Feda, J. (2002). Notes on the effect of grain crushing on the granular soil behaviour. *Engineering Geology*, 63(1), 93-98. https://doi.org/10.1016/S0013-7952(01)00072-2

Hall, C. D., Harrisberger, W. H. (1970). Stability of sand arches: a key to sand control. *Journal of Petroleum Technology*, 22(7), 821-829. https://doi.org/10.2118/2399-PA

Houseknecht, D. W. (1989). Assessing the relative importance of compaction processes and cementation to reduction of porosity in sandstones-reply. *Aapg Bulletin American Association of Petroleum Geologists*, 73 (10), 1277–1279. https://doi.org/10.1306/44B4AA1E-170A-11D7-8645000102C1865D

Huang, Z., Bai, Y., Xu, H., Cao, Y., & Hu, X. (2017). A theoretical model to predict the critical hydraulic gradient for soil grain movement under two-dimensional seepage flow. *Water*, 9(11), 828. https://doi.org/10.3390/w9110828

Huang, Z., Xu, H., Bai, Y., & Yang, S. (2019). A theoretical-empirical model to predict the saturated hydraulic conductivity of sand. *Soil Science Society of America Journal*, 83(1), 64-77. https://doi.org/10.2136/sssaj2017.09.0322

Hughes, P., Muessel, T. S. (2000). *Energy savings performance contracting-experience of the U.S. department of energy federal energy management program*. Paper presented at 2000 ACEEE Summer Studies on Energy Efficiency in Buildings, ashington D.C.

Huo, D., Benson, S. M. (2016). Experimental investigation of stress-dependency of relative permeability in rock fractures. *Transport in Porous Media*, 113(3), 567–590. https://doi.org/10.1007/s11242-016-0713-z

Israr, J., & Indraratna, B. (2019). Study of Critical Hydraulic Gradients for Seepage-Induced Failures in Granular Soils. *Journal of Geotechnical and Geoenvironmental Engineering*, 145(7), 04019025. https://doi.org/10.1061/(asce)gt.1943-5606.0002062

Katarzyna, S. (2006). Clogging microstructures in the vadose zone—laboratory and field studies. *Hydrogeology Journal*, 14(6), 1005-1007. https://doi.org/10.1007/s10040-006-0027-2

Kim, C., Lee, J. (2017). Experimental study on the variation of relative permeability due to clay minerals in low salinity water-flooding. *Petroleum Science and Engineering*, 151, 292–304. https://doi.org/10.1016/j.petrol.2017.01.014

Krumbein W. C., Monk G. D. (1943). Permeability as a function of size parameters of uncemented sand. *Transactions of the American Institute of Mining and Metallurgical Engineers*, 151, 153–163. https://doi.org/10.2118/943153-G

Lei, Z., Zhang, Y., Yu, Z., Hu, Z., Li, L., Zhang, S., & Xie, Y. (2019). Exploratory research into the enhanced geothermal system power generation project: The Qiabuqia geothermal field, Northwest China. *Renewable Energy*, 139, 52-70. https://doi.org/10.1016/j.renene.2019.01.088

Li, K., Bian, H., Liu, C., Zhang, D., Yang, Y. (2015). Comparison of geothermal with solar and wind power generation systems. *Renewable & Sustainable Energy Reviews*, 42, 1464–1474. https://doi.org/10.1016/j.rser.2014.10.049

Li, Y., Pan, J., Chen, X., Xue, S., Feng, J., Muhammad, T., & Zhou, B. (2019). Dynamic effects of chemical precipitates on drip irrigation system clogging using water with high sediment and salt loads. *Agricultural Water Management*, 213, 833-842. https://doi.org/10.1016/j.agwat.2018.11.021

Lior, N. (2008). Energy resources and use: The present situation and possible paths to the future. *Energy*, 33(6), 842-857. https://doi.org/10.1016/j.energy.2007.09.009

Lior, N. (2010). Energy resources and use: The present (2008) situation and possible sustainable paths to the future. *Energy*, 35(6), 2631-2638. https://doi.org/10.1016/j.energy.2009.06.049

Lund, H., 2009. *Renewable Energy System*, 2nd ed. San Diego, CA:Academic Press.

Masch, F. D., & Denny, K. J. (1966). Grain size distribution and its effect on the permeability of uncemented sands. *Water Resources Research*, 2(4), 665-677. https://doi.org/10.1029/WR002i004p00665

Nian, Y., & Cheng, W. (2018a). Insights into geothermal utilization of abandoned oil and gas wells. *Renewable & Sustainable Energy Reviews*, 87, 44-60. https://doi.org/10.1016/j.rser.2018.02.004

Nian, Y., & Cheng, W. (2018b). Evaluation of geothermal heating from abandoned oil wells. *Energy*,142, 592-607. https://doi.org/10.1016/j.energy.2017.10.062

Nian, Y., Cheng, W., Yang, X., & Xie, K. (2019). Simulation of a novel deep ground source heat pump system using abandoned oil wells with coaxial BHE. *International Journal of Heat and Mass Transfer*, 137, 400-412. https://doi.org/10.1016/j.ijheatmasstransfer.2019.03.136

Ozgurel, H. G., & Vipulanandan, C. (2005). Effect of Grain Size and Distribution on Permeability and Mechanical Behavior of Acrylamide Grouted Sand. *Journal of Geotechnical and Geoenvironmental Engineering*, 131(12), 1457-1465. https://doi.org/10.1061/(ASCE)1090-0241(2005)131:12(1457)

Pavelic, P., Dillon, P., Barry, K. E., Herczeg, A. L., Rattray, K. J., Hekmeijer, P., Gerges, N. Z. (1998). *Well clogging effects determined from mass balances and hydraulic response at a stormwater ASR site*. Paper presented at 3th International Symposium on Artificial Recharge, Amsterdam, Holland.

Pavelic, P., Dillon, P. J., Barry, K.E., Vanderzalm, J.L., Correll, R.L., Rinck-Pfeiffer, S.M. (2007). Water quality effects on clogging rates during reclaimed water ASR in a carbonate aquifer. *Journal of Hydrology*, 334, 1–16. https://doi.org/10.1016/j.jhydrol.2006.08.009

Pavelic, P., Dillon, P., Mucha, M., Nakai, T., Barry, K., & Bestland, E. A. (2011). Laboratory assessment of factors affecting soil clogging of soil aquifer treatment systems.. *Water Research*, 45(10), 3153-3163. https://doi.org/10.1016/j.watres.2011.03.027

Reddi, L. N., Xiao, M., Hajra, M. G., & Lee, I. M. (2005). Physical clogging of soil filters under constant flow rate versus constant head. *Canadian Geotechnical Journal*, 42(3), 804-811. https://doi.org/10.1139/t05-018

Rehg, K J, Packman, A I, Ren, J. (2005). Effects of suspended sediment characteristics and bed sediment transport in streambed clogging. *Hydrological Processes*, 19(2), 413 – 427. https://doi.org/10.1002/hyp.5540

Richards, K. S., & Reddy, K. R. (2012). Experimental investigation of initiation of backward erosion piping in soils. *Géotechnique*, 62(10), 933-942. https://doi.org/10.1680/geot.11.P.058

Rinck-Pfeiffer, S.M., Ragusa, S.R., Sztajnbok, P., Vandevelde, T. (2000). Interrelationships between biological, chemical and physical processes as an analog to clogging in aquifer storage and recovery (ASR) wells. *Water Research*, 34 (7), 2110–2118. https://doi.org/10.1016/S00431354(99)00356-5

Rosas, J., Lopez, O., Missimer, T. M., Coulibaly, K., Dehwah, A. H., Sesler, K., & Mantilla, D. (2014). Determination of Hydraulic Conductivity from Grain-Size Distribution for Different Depositional Environments. *Ground Wate*r, 52(3), 399-413. https://doi.org/10.1111/gwat.12078

Schutjens, P., De Ruig, H., Van Muster, J. G., Sayers, C. M., & Whitworth, J. L. (1996). Production-Induced Compaction of the Brent Field: An Experimental Approach. *Spe Formation Evaluation*, 11(02), 99-107. https://doi.org/10.2118/28096-PA

Sheng, G., Javadpour, F., & Su, Y. (2019). Dynamic porosity and apparent permeability in porous organic matter of shale gas reservoirs. *Fuel*, 251, 341-351. https://doi.org/10.1016/j.fuel.2019.04.044

Stáhl, G., Pátzay, G., Weiser, L., Kálmán, E. (2000). Study of calcite scaling and corrosion processes in geothermal systems. *Geothermics*, 29, 105–219. https://doi.org/10.1016/S0375-6505(99)00052-8

Su, Y., Yang, F., Wang, B., Jia, Z., & Duan, Z. (2018). Recharge of cooled water into sandstone geothermal reservoirs in China: a review. *Geosciences Journal*, 22(1), 199-207. https://doi.org/10.1007/s12303-017-0019-3

Suleiman, K.A., Swartzendruber, D. (2003). Measurement of sated hydraulic conductivity of surface soil in the field with a small-plot sprinkling infiltrometer. *Journal of Hydrology*, 272 (1), 203–212. https://doi.org/10.1016/S0022-1694(02)00265-2

Templeton, J. D., Ghoreishimadiseh, S. A., Hassani, F. P., & Alkhawaja, M. (2014). Abandoned petroleum wells as sustainable sources of geothermal energy. *Energy*, 70, 366-373. https://doi.org/10.1016/j.energy.2014.04.006

Torkzaban, S., Bradford, S. A., Vanderzalm, J., Patterson, B. M., Harris, B., & Prommer, H. (2015). Colloid release and clogging in porous media: Effects of solution ionic strength and flow rate. *Journal of Contaminant Hydrology*, 181, 161-171. https://doi.org/10.1016/j.jconhyd.2015.06.005

Tufenkji, N. (2007). Modeling microbial transport in porous media: traditional approaches and recent developments. *Advances in Water Resources*, 30, 1455-1469. https://doi.org/10.1016/j.advwatres.2006.05.014

Van Beek, C. G., Hubeek, A. A., Gonzalez, B. D., & Stuyfzand, P. J. (2017). Chemical and mechanical clogging of groundwater abstraction wells at well field Heel, the Netherlands. *Hydrogeology Journal*, 25(1), 67-78. https://doi.org/10.1007/s10040-016-1469-9

Van Beek, V. M., Bezuijen, A., Sellmeijer, J. B., & Barends, F. (2014). Initiation of backward erosion piping in uniform sands. *Géotechnique*, 64(12), 927-941. https://doi.org/10.1680/geot.13.P.210

Vandenboer, K., Dolphen, L., & Bezuijen, A. (2019). Backward erosion piping through vertically layered soils. *European Journal of Environmental and Civil Engineering*, 23(11), 1404-1412. https://doi.org/10.1080/19648189.2017.1373708

Wang, H., Su, Y., Zhao, Z., Wang, W., Sheng, G., & Zhan, S. (2019b). Apparent permeability model for shale oil transport through elliptic nanopores considering wall-oil interaction. *Journal of Petroleum Science and Engineering*, 176, 1041-1052. https://doi.org/10.1016/j.petrol.2019.02.027

Wang, J., & Qiu, Z. (2017b). Anisotropic hydraulic conductivity and critical hydraulic gradient of a crushed sandstone–mudstone grain mixture. *Marine Georesources & Geotechnology*, 35(1), 89-97. https://doi.org/10.1080/1064119X.2015.1103825

Wang, J., Zhuang, P., Luan, J., Liu, T., Tan, Y., & Zhang, J. (2019a). Estimation of unsaturated hydraulic conductivity of granular soils from grain size parameters. *Water*, 11(9), 1826. https://doi.org/10.3390/w11091826

Wang, S., Chen, J., Luo, Y., & Sheng, J. (2014). Experiments on internal erosion in sandy gravel foundations containing a suspended cutoff wall under complex stress states. *Natural Hazards*, 74(2), 1163-1178. https://doi.org/10.1007/s11069-014-1243-z

Wang, Y., Cui, Y., Tang, A. M., Benahmed, N., & Duc, M. (2017a). Effects of aggregate size on the compressibility and air permeability of lime-treated fine-grained soil. *Engineering Geology*, 228, 167-172. https://doi.org/10.1016/j.enggeo.2017.08.005

Wang, Y., Mingxin Huo, M., Li, Q., et al. (2018b). Comparison of clogging induced by organic and inorganic suspended grains in a porous medium: implications for choosing physical clogging indicators. *Journal of Soils and Sediments*, 18 (9), 2980-2994. https://doi.org/10.1007/ s11368-018-1967-6

Xia, L., Zheng, X., Shao, H., Xin, J., Peng, T. (2014). Influences of environmental factors on bacterial extracellular polymeric substances production in porous media. *Journal of Hydrology*, 519, 3153–3162. https://doi.org/10.1016/j.jhydrol.2014.10.045

Xia, L., Zheng, X., Shao, H., Xin, J., Sun, Z., Wang, L. (2016). Effects of bacterial cells and two types of extracellular polymers on bioclogging of sand columns. *Journal of Hydrology*, 535, 293–300. https://doi.org/10.1016/j.jhydrol.2016.01.075

Xian, Y., Jin, M. G., Zhan, H. B., Liu, Y.F. (2019). Reactive transport of nutrients and bioclogging during dynamic disconnection process of stream and groundwater. *Water Resources Research*, 55 (5), 3882–3903. https://doi.org/10.1029/2019WR024826

Xiong, Y., Xu, H., Wang, Y., Zhou, W., Liu, C., & Wang, L. (2018b). Fluid flow with compaction and sand production in uncemented sandstone reservoir. *Petroleum*, 4(3), 358-363. https://doi.org/10.1016/j.petlm.2018.05.003

Xiong, Y., Xu, H., Wang, Y., Zhou, W., Wang, L., Feng, K. (2018a). The variation mechanism of petrophysical properties and the effect of compaction on the relative permeability of an uncemented sandstone reservoir. *Marine and Petroleum Geology*, (92), 754-763. https://doi.org/10.1016/j.marpetgeo.2017.12.006

Xu, Z. Q., Wu, Y. Q., Wu, J. Z., et al. (2011). A model of seepage field in the tailings dam considering the chemical clogging process. *Advances in Engineering Software*, 42(7), 426 – 434. https://doi.org/10.1016/j.advengsoft.2011.03.009

Xu, Z., Yang, X., Chai, J., Qin, Y., & Li, Y. (2016). Permeability characteristics of tailings considering chemical and physical clogging in lixi tailings dam, China. *Journal of Chemistry*, 2016, 1-8. https://doi.org/10.1155/2016/8147845

Yang, F. J., Hu, D. W., Tian Z. B., Zhou H., Lu J. J., Luo Y. J., Gui S. Q. (2019). Evolution and mechanism of permeability of uncemented sandstone under the compaction of a high hydrostatic pressure. *Rock and Soil Mechaniacs*, 41(1), 1-13. (in Chinese) https://doi.org/10.16285/j.rsm.2018.2279

Ye, S., Sleep, B.E., Chien, C. (2009). The impact of methanogenesis on flow and transport in coarse sand. *Journal of Contaminant Hydrology*, 103, 48–57. https://doi.org/10.1016/j.jconhyd.2008.09.004

Zhao, Y., Feng, Z., Xi, B. (2015). Deformation and instability failure of borehole at high temperature and high pressure in hot dry rock exploitation. *Renewable Energy*, 77(1), 159–165. https://doi.org/10.1016/j.renene.2014.11.086

Zheng T., Zheng X., Sun Q., Wang L., Walther M. (2020). Insights of variable permeability full-section wall for enhanced control of seawater intrusion and nitrate contamination in unconfined aquifers. *Journal of Hydrology,*586, 124831. https://doi.org/10.1016/j.jhydrol.2020.124831

Zhu, J., Hu, K., Lu, X., Huang, X., Liu, K., & Wu, X. (2015). A review of geothermal energy resources, development, and applications in China: Current status and prospects. *Energy*, 93, 466-483. https://doi.org/10.1016/j.energy.2015.08.098

Zivar, D., Shad, S., Foroozesh, J., & Salmanpour, S. (2019). Experimental study of sand production and permeability enhancement of uncemented rocks under different stress conditions. *Journal of Petroleum Science and Engineering*, 181: 106238. https://doi.org/10.1016/j.petrol.2019.106238